

# Optically tunable nonlinear mechanical damping in an optomechanical resonator

Hideki Arahari,\* Motoki Asano,† Hiroshi Yamaguchi, and Hajime Okamoto  
*Basic Research Laboratories, NTT, Inc., 3-1 Morinosato Wakamiya, Atsugi-shi, Kanagawa 243-0198 Japan*  
(Dated: February 9, 2026)

We theoretically propose and experimentally demonstrate optically tunable nonlinear mechanical damping in a cavity optomechanical system utilizing a partly resolved sideband regime. Optomechanical coupling provides a delayed nonlinear backaction to the mechanical modes, resulting in nonlinear mechanical damping. This optically induced nonlinear damping is observed in the frequency and time domains, and we show using both theory and experiment that it can be tuned via laser detuning. We also observe optically mediated cross-nonlinear damping between two mechanical modes: the amplitude of one mode modulates the damping of the other. The presented results show a fully tunable scheme of nonlinear mechanical damping that will be applicable to various non-trivial systems, governed by nonlinear, nonequilibrium, and non-Hermitian phenomena.

*Introduction* - Nonlinear damping, where the rate of energy dissipation depends on the system dynamics, is a ubiquitous phenomenon that appears across a wide range of oscillatory systems including ship dynamics [1, 2], electrical circuits [3], and biological rhythms [4]. Beyond such macroscopic examples, nonlinear damping also plays a significant role in well-engineered mesoscale platforms such as mechanical resonators [5–17], superconducting circuits [18], and nanomagnets [19]. In these systems, amplitude-dependent dissipation governs key dynamical behaviors including self-stabilization of oscillation amplitudes [17], intermodal coupling [14], and dissipative reservoir engineering for tailoring quantum states [18].

At a phenomenological level, nonlinear damping is often captured by a cubic friction term, as exemplified by the van der Pol equation [20]. Over the past decade, substantial progress has been made toward elucidating microscopic mechanisms underlying nonlinear damping in mesoscale devices and this has clarified how effective nonlinear damping emerge from device geometry, material properties, and mode coupling [14, 15, 21]. However, in most existing platforms, such nonlinear damping is intrinsically fixed once the system is fabricated rendering it difficult to tune *in situ*. This lack of controllability has hindered systematic exploration of nonlinear dissipation as a universal nonequilibrium resource, which limits access to phenomena such as dissipative phase transitions [22], parity-time symmetric dynamics [23, 24], and collective nonequilibrium dynamics stabilized by irreversible phase-space flows [25].

Here we demonstrate optically tunable nonlinear mechanical damping arising from delayed optical backaction in a cavity optomechanical system. In a partly resolved sideband regime where the cavity response time is comparable to the mechanical oscillation period, nonlinear damping is selectively tuned by laser detuning. We identify the physical origin of this effect as a competition between mechanical motion and the finite cavity response. We further extend this framework to multiple mechanical modes and experimentally reveal optically mediated cross-nonlinear damping as a purely dissipative interac-

tion. These results establish cavity optomechanics as a versatile platform for engineering nonlinear dissipation and nonequilibrium mechanical dynamics.

*Theoretical model* - Optomechanical coupling induces mechanical nonlinearity through a nonlinear backaction force, whereby a strong optical field reflects forces containing higher-order terms in the mechanical displacement [26–28]. Such a nonlinear backaction force can acquire a non-conservative component - namely, nonlinear damping - when the cavity conditions are tuned to introduce a finite delay, as shown in Fig. 1(a). The magnitude of this delay is governed by resolved sideband parameter  $\kappa_{\text{cav}}/\Omega_m$  where  $\kappa_{\text{cav}}$  and  $\Omega_m$  denote the optical cavity dissipation rate and mechanical resonance frequency, respectively. However, conventional theories typically assume the adiabatic limit,  $\kappa_{\text{cav}}/\Omega_m \gg 1$  [27, 28]. To evaluate quantitatively the nonlinear delayed backaction forces induced by the optical cavity field, we need to extend the theoretical framework.

We theoretically quantify nonlinear backaction effects on the  $j$ th mechanical mode,  $b_j$  ( $j = 1, 2, \dots, N$ ), induced by an optical cavity field using a complex-amplitude description under the rotating-wave approximation. The equations of motion for both optical and mechanical amplitudes,  $a(t)$  and  $b_j(t)$ , are, respectively, given by

$$\dot{a}(t) = \left[ i\Delta - \frac{\kappa_{\text{cav}}}{2} \right] a(t) + i \sum_{j=1}^N g_j a(t) (b_j(t) + b_j^*(t)) + \sqrt{\kappa_{\text{in}}} a_{\text{in}}, \quad (1)$$

$$\dot{b}_j(t) = -i\Omega_j b_j(t) - \frac{\Gamma_j}{2} b_j(t) + ig_j |a(t)|^2. \quad (2)$$

Here,  $\Delta$  is the laser detuning from the cavity resonance,  $\kappa_{\text{cav}}$  is the total cavity decay rate, and  $\kappa_{\text{in}}$  is the coupling rate to input optical field  $a_{\text{in}}$ . For the  $j$ th mechanical mode,  $\Omega_j$ ,  $\Gamma_j$ , and  $g_j$  denote the resonance frequency, damping rate, and optomechanical coupling rate, respectively. A general formulation of nonlinear optomechanical backaction is obtained by formally solving Eq. (1)

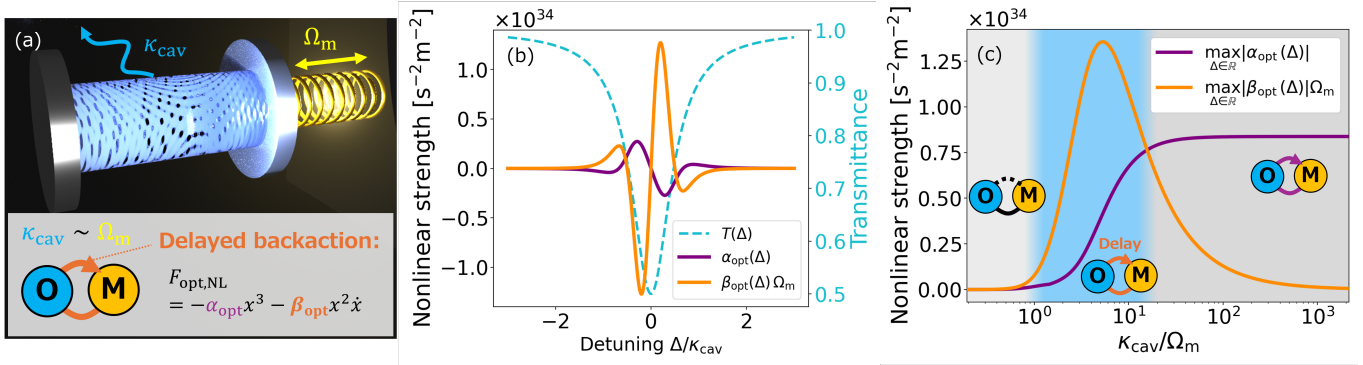


FIG. 1. (a) Concept of nonlinear mechanical damping induced by delayed backaction in cavity optomechanics, where cavity decay rate  $\kappa_{\text{cav}}$  becomes comparable to mechanical frequency  $\Omega_m$ . (b) Theoretical detuning dependence of the mechanical nonlinearities near cavity resonance. The orange curve shows nonlinear damping strength  $\beta_{\text{opt}}(\Delta)\Omega_m$  and the purple curve represents Duffing nonlinearity  $\alpha_{\text{opt}}(\Delta)$ . The light-blue dashed line indicates the optical cavity transmittance. (c) Theoretically calculated maximum strength of the nonlinearities optimized over detuning  $\Delta$  as a function of  $\kappa_{\text{cav}}/\Omega_m$ . The orange curve represents maximum nonlinear damping strength  $\max_{\Delta \in \mathbb{R}} |\beta_{\text{opt}}(\Delta)|\Omega_m$  and the purple curve shows maximum Duffing nonlinearity  $\max_{\Delta \in \mathbb{R}} |\alpha_{\text{opt}}(\Delta)|$ . Schematic illustrations highlight the distinct optomechanical backaction mechanisms in different parameter regimes. All calculations use parameters corresponding to the employed experimental system (a microbottle optomechanical resonator, as discussed later in Fig. 2) assuming an input optical power of 50 mW.

in the time-domain integral form expanding the solution to include higher-order perturbative contributions. This procedure incorporates the history of the mechanical motion into the radiation-pressure response through a memory kernel, yielding an explicit third-order expression for the optically induced nonlinearities [see Supplemental Material for details]. For simplicity, here we show the equation of motion for single mechanical mode  $N = 1$  given by

$$\dot{b} = -i \left( \Omega_{\text{eff}} - i \frac{\Gamma_{\text{eff}}}{2} \right) b - i \left( \frac{3\alpha_{\text{opt}}}{2\Omega_m} - i \frac{\beta_{\text{opt}}}{2} \right) x_{\text{zpf}}^2 |b|^2, \quad (3)$$

where  $\Omega_{\text{eff}}$  and  $\Gamma_{\text{eff}}$ , respectively, denote the effective mechanical resonance frequency and damping modified by linear optomechanical backaction, and  $x_{\text{zpf}}$  is the zero-point fluctuation amplitude of the mechanical oscillator. The equation includes both real and imaginary contributions of the nonlinear backaction force with the coefficients of  $\alpha_{\text{opt}}$  and  $\beta_{\text{opt}}$ , respectively, with the imaginary part representing optically induced nonlinear damping. Each coefficient explicitly depends on the detuning, as follows:

$$\alpha_{\text{opt}}(\Delta) = \frac{2\Omega_m}{3} \frac{n_{\text{cav}}(\Delta)g^4}{x_{\text{zpf}}^2} \text{Re}[C(\Delta)], \quad (4)$$

$$\beta_{\text{opt}}(\Delta) = -2 \frac{n_{\text{cav}}(\Delta)g^4}{x_{\text{zpf}}^2} \text{Im}[C(\Delta)], \quad (5)$$

$$C(\Delta) = i [S_+(\Delta) - S_-^*(\Delta)], \quad (6)$$

$$S_{\pm}(\Delta) = \chi_{\pm}\chi_0\chi_{\mp} + (\chi_{\pm})^2\chi_0 + (\chi_{\pm})^2\chi_{\pm 2} + \chi_{\mp}\chi_{\mp 2}^*\chi_{\mp}^* + \chi_{\pm}\chi_0^*(\chi_{\pm} + \chi_{\mp})^*. \quad (7)$$

Here,  $n_{\text{cav}}(\Delta) = \kappa_{\text{in}}|a_{\text{in}}|^2|\chi_0(\Delta)|^2$  denotes the bare intracavity photon number, and  $\chi_{\pm n} = (\kappa_{\text{cav}}/2 - i(\Delta \pm n\Omega_m))^{-1}$  describes the first-order optomechanical susceptibility, where  $n$  is an integer.

We first examine the detuning dependence of  $\alpha_{\text{opt}}(\Delta)$  and  $\beta_{\text{opt}}(\Delta)$  for  $\kappa_{\text{cav}}/\Omega_m = 4.0$  [see Fig. 1(b)]. At this parameter, the nonlinear damping clearly dominates the Duffing nonlinearity across a wide detuning range. In terms of their detuning dependence, similar to the first-order backaction effect, *e.g.*, optical spring effect, both coefficients attain their maxima near the slope of the cavity resonance. Notably, enhanced positive nonlinear damping emerges on the blue-detuned side, which is readily accessible experimentally even in the presence of photothermal effects [29]. We then evaluate  $\max_{\Delta \in \mathbb{R}} |\alpha_{\text{opt}}(\Delta)|$  and  $\max_{\Delta \in \mathbb{R}} |\beta_{\text{opt}}(\Delta)|\Omega_m$  as functions of resolved sideband parameter  $\kappa_{\text{cav}}/\Omega_m$  to identify the conditions for observing optically induced nonlinear damping [Fig. 1(c)]. In adiabatic regime  $\kappa_{\text{cav}}/\Omega_m \gg 1$ , the mechanical nonlinearity is predominantly Duffing-like, as the delayed backaction becomes negligible. In contrast, when  $\kappa_{\text{cav}}$  becomes comparable to  $\Omega_m$ , the mechanical nonlinearity is dominated by nonlinear damping, reflecting the emergence of nonlinear damping induced by the finite backaction delay through the optical cavity. For non-adiabatic limit  $\kappa_{\text{cav}}/\Omega_m \ll 1$ , the backaction effect is suppressed because the optical cavity cannot respond to variations in the mechanical modes.

*Nonlinear damping in a single mechanical mode* - The optically induced nonlinear damping reported here arises generically in cavity optomechanical resonators operated in the partly resolved sideband regime,  $\kappa_{\text{cav}} \sim \Omega_m$ . As a concrete experimental actualization, we employ a microbottle optomechanical resonator fabricated on a silica

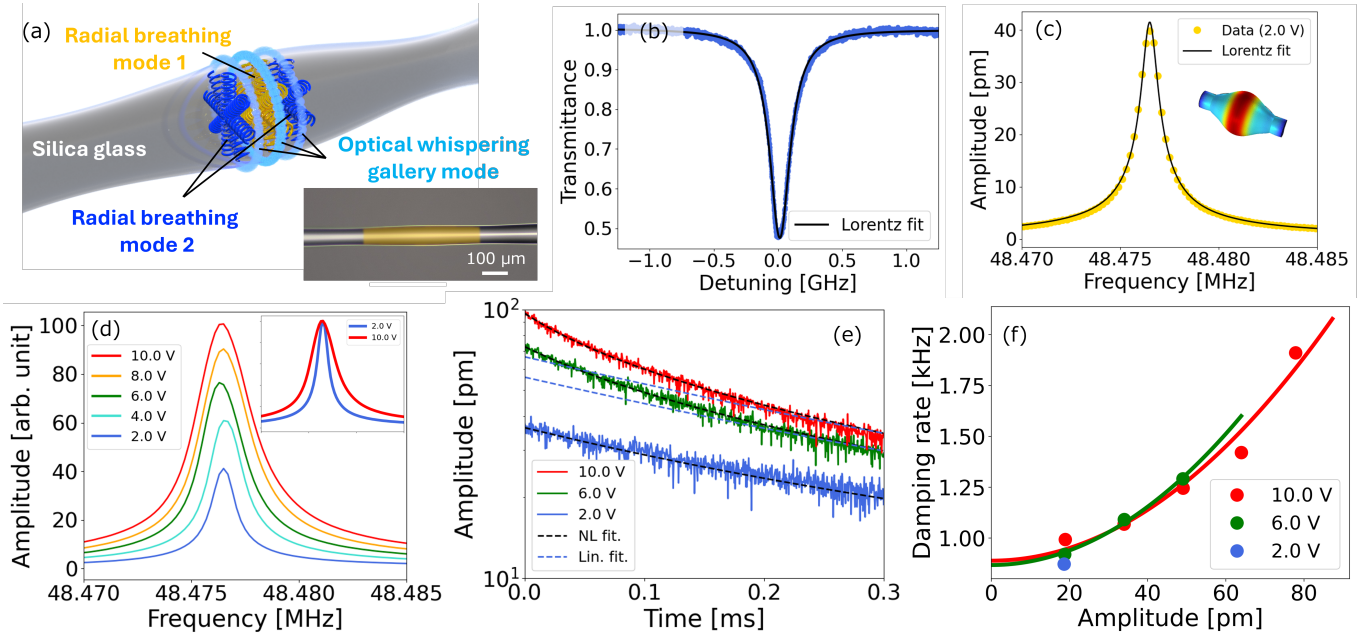


FIG. 2. (a) Schematic of microbottle optomechanical resonator and its optical micrograph, in which the bottle region is highlighted in light yellow. Two representative radial breathing modes are illustrated, anticipating the multimode discussion in Fig. 4. (b) Optical transmission spectrum (at  $\lambda = 1.55 \mu\text{m}$ ) with a Lorentzian fit yielding  $\kappa_{\text{cav}}/2\pi = 194 \text{ MHz}$  ( $Q_{\text{cav}} = 1.0 \times 10^6$ ). (c) Mechanical resonance spectrum of a representative radial breathing mode (RBM) under weak excitation with a Lorentzian fit yielding  $\Gamma_m/2\pi = 0.83 \text{ kHz}$  at  $\Omega_m/2\pi = 48.476 \text{ MHz}$ . (d) Mechanical resonance spectra at different excitation strengths parameterized by the voltage applied to the EOM,  $V_{\text{EOM}}$ . Inset: Corresponding normalized spectra at 10.0 V and 2.0 V. (e) Ring-down traces for different drive strengths. Black dashed curves show nonlinear-damping fits while blue dashed curves show linear-damping fits. (f) Damping rate versus oscillation amplitude, exhibiting quadratic scaling consistent with cubic nonlinear damping. Fit yields the linear damping rate,  $\Gamma_0/2\pi = 0.89 \text{ kHz}$ , and  $\beta_{\text{opt}}/2\pi = 6.2 \times 10^{23} \text{ Hz/m}^2$ . The absolute amplitude is calibrated from the thermal motion of the RBM using effective mass  $m_{\text{eff}} \simeq 7 \times 10^{-9} \text{ kg}$  (See Supplemental Material for details).

fiber via the heat-and-pull technique [30–33]. The resonator supports a dense spectrum of optical whispering-gallery modes (WGMs) with various  $Q$  values, enabling the selective excitation of a specific optical resonance with a desired value of  $\kappa_{\text{cav}}$  and thereby providing a versatile platform for accessing  $\kappa_{\text{cav}} \sim \Omega_m$ . The maximum diameter, neck diameter, and the length between the two necks of the microbottle were  $80 \mu\text{m}$ ,  $70 \mu\text{m}$ , and  $450 \mu\text{m}$ , respectively, as shown in Fig. 2(a). To couple laser light evanescently into an optical WGM, a tapered optical fiber with the diameter of approximately  $1.5 \mu\text{m}$  was brought into contact with the resonator. By scanning the laser frequency and measuring the transmission spectra of the optical WGMs, we obtained high- $Q$  resonances with optical quality factors  $Q_{\text{opt}} \sim 10^6$  [see Fig. 2(b) for a representative spectrum].

The nonlinear mechanical damping was investigated in the radial breathing modes (RBMs) of the microbottle resonator. We emphasize that the RBMs exhibit negligible geometric nonlinearity because their displacement amplitudes (in the order of picometers) are much smaller than the device dimensions (sub-mm diameter). The geometric Duffing coefficient,  $\alpha_{\text{geo}}$ , is estimated in the

Supplemental Material and is more than eight orders of magnitude smaller than the optically induced Duffing coefficient,  $\alpha_{\text{opt}}$ .

To observe mechanical resonance characteristics, two lasers at wavelengths of 1550 nm (pump) and 1520 nm (probe) were simultaneously injected into different optical modes. The pump laser, with a power of approximately 50 mW, serves two roles: it induces optomechanical nonlinearity and drives the mechanical modes via intensity modulation using an electro-optic modulator (EOM). The probe laser was tuned to the slope of an optical resonance to measure independently the mechanical vibration using a lock-in amplifier. All experiments were performed at ambient pressure and room temperature. The configuration details are given in the Supplemental Material. Figure 2(c) shows the measured frequency response of the RBMs, with the resonance frequency of approximately 48.5 MHz and the mechanical damping rate of  $\Gamma_m/2\pi = 0.83 \text{ kHz}$ , in agreement with previous reports [28, 32, 34]. Under these conditions, the resolved sideband parameter is  $\kappa_{\text{cav}}/\Omega_m \simeq 4.0$ , where nonlinear damping dominates, which is consistent with Fig. 1(c).

To verify the emergence of nonlinear mechanical damping, we observed both the frequency and temporal responses with respect to the mechanical drive strength, *i.e.*, the applied radio-frequency (RF) voltage to the EOM,  $V_{\text{EOM}}$ . Figure 2(d) shows the mechanical resonance spectra measured using lock-in detection at different  $V_{\text{EOM}}$  values. As the excitation strength increases, the resonance linewidth increases markedly, with the oscillation amplitude growing, which is a clear sign of nonlinear mechanical damping. In addition to the frequency responses, ring-down measurements were performed to measure directly the mechanical decay rate as a function of oscillation amplitude. An RF voltage in the form of a square pulse was applied to the EOM, and we directly measured the photodetector output without a lock-in to avoid additional signal fluctuations introduced by the amplifier process. The resulting signal exhibited exponential-like tails corresponding to the mechanical decay as shown in Fig. 2(e). At weak excitation (blue trace) the decay is purely exponential with a constant slope; from this slope the mechanical dissipation rate was estimated to be 0.89 kHz. Under stronger excitation (green and red traces) the decay becomes faster at large amplitudes and slower at small amplitudes, which is clear evidence of nonlinear damping. From the profile under the strongest excitation (red trace), we extracted the dissipation rate as a function of the amplitude [see Fig. 2(f)]. We obtain the maximum dissipation rate of  $\Gamma_{\text{max}}/2\pi = 1.9$  kHz, which is more than twice the intrinsic rate,  $\Gamma_0/2\pi = 0.89$  kHz, estimated from the intercept of the figure. The damping rate scales quadratically with the amplitude, which confirms a cubic nonlinear damping force. Thus, fitting the dissipation rate to a quadratic function yields nonlinear damping strength  $\beta_{\text{opt}}\Omega_m = 1.2 \times 10^{33} \text{ s}^{-2}\text{m}^{-2}$ . This value shows quantitative agreement within an order of magnitude with the theoretical estimate for  $\beta_{\text{opt}}\Omega_m$  shown in Fig. 1(b).

To assess whether the damping enhancement observed in Fig. 2 originates from optically induced nonlinear damping, we compare the experimentally measured damping change with the calculated detuning dependence based on the theoretically estimated nonlinear damping coefficient. Figure 3 shows the change in mechanical damping as a function of laser detuning. Note that only blue-detuned conditions are shown, since red-detuned conditions are experimentally inaccessible due to thermal instability under strong pumping. The experimental data, extracted from the linewidth increase between weak and strong excitation, exhibit a pronounced detuning dependence. As shown by the orange curve in Fig. 3, the measured damping change quantitatively follows the calculated detuning dependence obtained using the theoretically estimated nonlinear damping coefficient. This agreement demonstrates that the observed damping enhancement is well explained by optically induced nonlinear damping rather than by intrinsic geometric non-

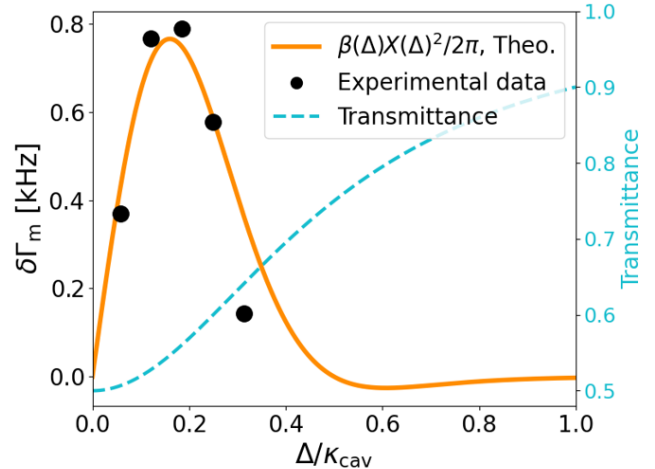


FIG. 3. Mechanical damping change as a function of laser detuning. The plots show the experimentally measured damping change extracted from the linewidth difference between strong and weak excitation ( $V_{\text{EOM}} = 9.0$  and 3.0 V). The orange curve represents the calculated damping increase using the theoretically estimated nonlinear damping coefficient [orange curve in Fig. 1(b)]. The calculation is calibrated using a detuning-dependent radiation-pressure drive expressed through oscillation amplitude  $X(\Delta)$ , which scales with the intracavity photon number as  $X(\Delta) \propto n_{\text{cav}}(\Delta)$ . The light-blue dashed line represents the optical cavity resonance as shown in Fig. 1(b).

linearities. Consistently, geometrical nonlinearity  $\alpha_{\text{geo}}$  is estimated to be much smaller than the optomechanical one,  $\alpha_{\text{geo}} \ll \alpha_{\text{opt}}$ . As a consequence of this detuning dependence, nonlinear damping terms can be selectively enhanced or suppressed by tuning the laser detuning, which enable engineered mechanical nonlinearities through optical control.

*Cross-nonlinear damping between two mechanical modes* - Because the nonlinear damping is mediated by the common optical cavity field, multiple mechanical modes coupled to the same optical mode as illustrated in Fig. 2(a) can be interconnected through nonlinear mechanical damping. Thus, when the amplitude of one mechanical mode increases, the other mode can be strongly damped. This effect is referred to as cross-nonlinear damping [see Fig. 4(a)]. Here, we observed cross-nonlinear mechanical damping between two RBMs with resonance frequencies of 48.0 MHz (probe mode) and 48.5 MHz (control mode). We tuned the optical mode so that it couples simultaneously to both RBMs. Figure 4(b) shows temporal ring-down traces of the probe mode with (red) and without (blue) excitation of the control mode. The decay time changed from 0.159 ms (2.00 kHz, without excitation) to 0.121 ms (2.62 kHz, with excitation), which constitutes clear evidence of cross-nonlinear mechanical damping. Moreover, we measured the mechanical damping rate of the probe

mode, denoted by  $\Gamma_{\text{pro}}$ , while finely varying the excitation amplitudes of the control and probe modes [see Fig. 4(c)]. Damping rate  $\Gamma_{\text{pro}}/2\pi$  increased gradually to 2.62 kHz as we increased the excitation of the control mode (via cross-nonlinear damping) and the probe mode itself (via the self-nonlinear damping reported in Fig. 2). Based on this, the cross-nonlinear damping coefficient,  $\beta_{\text{cross}}/2\pi$ , was estimated to be  $2.1 \times 10^{23}$  Hz/m<sup>2</sup>, showing agreement in order of magnitude with the theoretical estimate.

We developed the theoretical framework for nonlinear damping induced by delayed optomechanical backaction, and experimentally demonstrated optically tunable nonlinear damping in an optomechanical resonator. These results reveal the mechanism that generates nonlinear mechanical damping and they show that its strength can be tuned by laser detuning. The optically tunable nonlinear mechanical damping offers three potential advantages. (1) The strength of the nonlinear mechanical damping can be tuned on demand and is independent of material composition and geometric design [21]. This capability enables systematic exploration of tunable nonlinear dynamics governed by nonlinear damping, in close analogy to Duffing nonlinearities, which have recently opened access to a variety of topological phenomena [35]. Furthermore, the proposed scheme can be extended to dynamic control of decay dynamics by tailoring the laser power or detuning injected into the cavity, opening a route to optomechanical Floquet engineering [28, 36, 37] of dissipation and the associated nonequilibrium dynamics [38]. (2) RBMs can reach frequencies of several gigahertz not only in WGM optomechanical resonators [39] but also in photonic crystal cavities [40]. In contrast to earlier experiments based on flexural modes, optomechanical schemes exploiting RBMs operate at much higher frequencies, providing a strong advantage for fast damping control. Moreover, high-frequency breathing modes are significantly less affected by air viscous damping, thereby simplifying the experimental configuration under ambient conditions. (3) Cross-nonlinear mechanical damping can be extended to multiple mechanical modes. Because optomechanical systems (including the microbottle resonators herein) scale well with the number of mechanical modes [34, 41], cross-nonlinear damping can be engineered by designing the optomechanical couplings.

We have shown nonlinear mechanical damping mediated by the optical cavity field. The nonlinear optomechanical coupling not only induces self-nonlinear damping but also allows its magnitude to be tuned via laser detuning. Furthermore, we observed an optically mediated cross-nonlinear damping effect by coupling a single optical mode to two mechanical modes. This advantageous optomechanical scheme will significantly accelerate studies of nonlinear and nonequilibrium dynamics assisted by nonlinear damping.

This work was supported by JSPS KAKENHI grant numbers JP23H05463.

\* hideki.arahari@ntt.com; These authors contributed equally to this work

† motoki.asano@ntt.com; These authors contributed equally to this work

- [1] M. Taylan, The effect of nonlinear damping and restoring in ship rolling, *Ocean engineering* **27**, 921 (2000).
- [2] Y. Yang, J. Du, H. Liu, C. Guo, and A. Abraham, A trajectory tracking robust controller of surface vessels with disturbance uncertainties, *IEEE Transactions on Control Systems Technology* **22**, 1511 (2013).
- [3] M. L. Cartwright, Balthazar van der Pol, *J. London Math. Soc* **35**, 367 (1960).
- [4] R. FitzHugh, Impulses and physiological states in theoretical models of nerve membrane, *Biophysical Journal* **1**, 445 (1961).
- [5] E. Buks and B. Yurke, Mass detection with a nonlinear nanomechanical resonator, *Physical Review E—Statistical, Nonlinear, and Soft Matter Physics* **74**, 046619 (2006).
- [6] R. Lifshitz and M. C. Cross, Nonlinear dynamics of nanomechanical and micromechanical resonators, in *Reviews of Nonlinear Dynamics and Complexity* (Wiley-VCH Verlag GmbH & Co. KGaA, 2009) pp. 1–52.
- [7] S. Zaitsev, O. Shtempluck, E. Buks, and O. Gottlieb, Nonlinear damping in a micromechanical oscillator, *Nonlinear Dynamics* **67**, 859 (2012).
- [8] M. Imboden, O. A. Williams, and P. Mohanty, Observation of nonlinear dissipation in piezoresistive diamond nanomechanical resonators by heterodyne down-mixing, *Nano Letters* **13**, 4014 (2013).
- [9] A. Eichler, J. Moser, J. Chaste, M. Zdrojek, I. Wilson-Rae, and A. Bachtold, Nonlinear damping in mechanical resonators made from carbon nanotubes and graphene, *Nature Nanotechnology* **6**, 339 (2011).
- [10] J. Güttinger, A. Noury, P. Weber, A. M. Eriksson, C. Lagoin, J. Moser, C. Eichler, A. Wallraff, A. Isacsson, and A. Bachtold, Energy-dependent path of dissipation in nanomechanical resonators, *Nature Nanotechnology* **12**, 631 (2017).
- [11] V. Singh, O. Shevchuk, Y. M. Blanter, and G. A. Steele, Negative nonlinear damping of a multilayer graphene mechanical resonator, *Physical Review B* **93**, 245407 (2016).
- [12] S. Yanai, V. Singh, M. Yuan, M. Gely, S. Bosman, and G. Steele, Mechanical dissipation in more superconducting metal drums, *Applied Physics Letters* **110**, 083103 (2017).
- [13] X. Dong, M. Dykman, and H. Chan, Strong negative nonlinear friction from induced two-phonon processes in vibrational systems, *Nature Communications* **9**, 3241 (2018).
- [14] L. Catalini, Y. Tsaturyan, and A. Schliesser, Soft-clamped phononic dimers for mechanical sensing and transduction, *Physical Review Applied* **14**, 014041 (2020).
- [15] L. Catalini, M. Rossi, E. C. Langman, and A. Schliesser, Modeling and observation of nonlinear damping in dissipation-diluted nanomechanical resonators, *Physical*

Review Letters **126**, 174101 (2021).

[16] A. Keşkekler, O. Shoshani, M. Lee, H. S. van der Zant, P. G. Steeneken, and F. Alijani, Tuning nonlinear damping in graphene nanoresonators by parametric-direct internal resonance, *Nature communications* **12**, 1099 (2021).

[17] J. M. Miller, A. Gomez-Franco, D. D. Shin, H.-K. Kwon, and T. W. Kenny, Amplitude stabilization of micromechanical oscillators using engineered nonlinearity, *Physical Review Research* **3**, 033268 (2021).

[18] M. F. Gely, A. Sanz Mora, S. Yanai, R. Van der Spek, D. Bothner, and G. A. Steele, Apparent nonlinear damping triggered by quantum fluctuations, *Nature Communications* **14**, 7566 (2023).

[19] I. Barsukov, H. Lee, A. Jara, Y.-J. Chen, A. Gonçalves, C. Sha, J. Katine, R. Arias, B. Ivanov, and I. Krivorotov, Giant nonlinear damping in nanoscale ferromagnets, *Science Advances* **5**, eaav6943 (2019).

[20] B. Van der Pol, Lxxviii. on “relaxation-oscillations”, *The London, Edinburgh, and Dublin Philosophical Magazine and Journal of Science* **2**, 978 (1926).

[21] J. Atalaya, T. W. Kenny, M. Roukes, and M. Dykman, Nonlinear damping and dephasing in nanomechanical systems, *Physical Review B* **94**, 195440 (2016).

[22] M. Dykman, Critical exponents in metastable decay via quantum activation, *Physical Review E—Statistical, Nonlinear, and Soft Matter Physics* **75**, 011101 (2007).

[23] S. Karthiga, V. Chandrasekar, M. Senthilvelan, and M. Lakshmanan, Twofold PT symmetry in nonlinearly damped dynamical systems and tailoring pt regions with position-dependent loss-gain profiles, *Physical Review A* **93**, 012102 (2016).

[24] H. Ramezani, T. Kottos, R. El-Ganainy, and D. N. Christodoulides, Unidirectional nonlinear pt-symmetric optical structures, *Physical Review A—Atomic, Molecular, and Optical Physics* **82**, 043803 (2010).

[25] U. Seifert, Stochastic thermodynamics, fluctuation theorems and molecular machines, *Reports on progress in physics* **75**, 126001 (2012).

[26] M. Aspelmeyer, T. J. Kippenberg, and F. Marquardt, Cavity optomechanics, *Reviews of Modern Physics* **86**, 1391 (2014).

[27] C. C. Rodrigues, C. M. Kersul, A. G. Primo, M. Lipson, T. P. Alegre, and G. S. Wiederhecker, Optomechanical synchronization across multi-octave frequency spans, *Nature Communications* **12**, 5625 (2021).

[28] M. Asano, H. Okamoto, and H. Yamaguchi, Synthesized Kuramoto potential via optomechanical Floquet engineering, *Science Advances* **11**, eady4167 (2025).

[29] T. Carmon, L. Yang, and K. J. Vahala, Dynamical thermal behavior and thermal self-stability of microcavities, *Optics express* **12**, 4742 (2004).

[30] M. Sumetsky, Whispering-gallery-bottle microcavities: the three-dimensional etalon, *Optics Letters* **29**, 8 (2004).

[31] M. Pöllinger, D. O’Shea, F. Warken, and A. Rauschenbeutel, Ultrahigh-Q tunable whispering-gallery-mode microresonator, *Physical Review Letters* **103**, 053901 (2009).

[32] M. Asano, Y. Takeuchi, W. Chen, S. K. Özdemir, R. Ikuta, N. Imoto, L. Yang, and T. Yamamoto, Observation of optomechanical coupling in a microbottle resonator, *Laser & Photonics Reviews* **10**, 603 (2016).

[33] A. MacDonald, B. Hauer, X. Rojas, P. Kim, G. Popowich, and J. Davis, Optomechanics and thermometry of cryogenic silica microresonators, *Physical Review A* **93**, 013836 (2016).

[34] M. Asano, H. Yamaguchi, and H. Okamoto, Free-access optomechanical liquid probes using a twin-microbottle resonator, *Science Advances* **8**, eabq2502 (2022).

[35] G. Villa, J. Del Pino, V. Dumont, G. Rastelli, M. Michałek, A. Eichler, and O. Zilberberg, Topological classification of driven-dissipative nonlinear systems, *Science Advances* **11**, eadt9311 (2025).

[36] L. Mercadé, K. Pelka, R. Burgwal, A. Xuereb, A. Martínez, and E. Verhagen, Floquet phonon lasing in multimode optomechanical systems, *Physical Review Letters* **127**, 073601 (2021).

[37] K. Pelka, G. Madiot, R. Braive, and A. Xuereb, Floquet control of optomechanical bistability in multimode systems, *Physical Review Letters* **129**, 123603 (2022).

[38] N. Sinitzyn, The stochastic pump effect and geometric phases in dissipative and stochastic systems, *Journal of Physics A: Mathematical and Theoretical* **42**, 193001 (2009).

[39] L. Ding, C. Baker, P. Senellart, A. Lemaitre, S. Ducci, G. Leo, and I. Favero, High frequency gaas nano-optomechanical disk resonator, *Physical Review Letters* **105**, 263903 (2010).

[40] M. Eichenfield, J. Chan, R. M. Camacho, K. J. Vahala, and O. Painter, Optomechanical crystals, *Nature* **462**, 78 (2009).

[41] M. Asano, H. Yamaguchi, and H. Okamoto, Fiber-type optomechanical array using high-Q microbottle resonators, *Physical Review Applied* **21**, 024013 (2024).

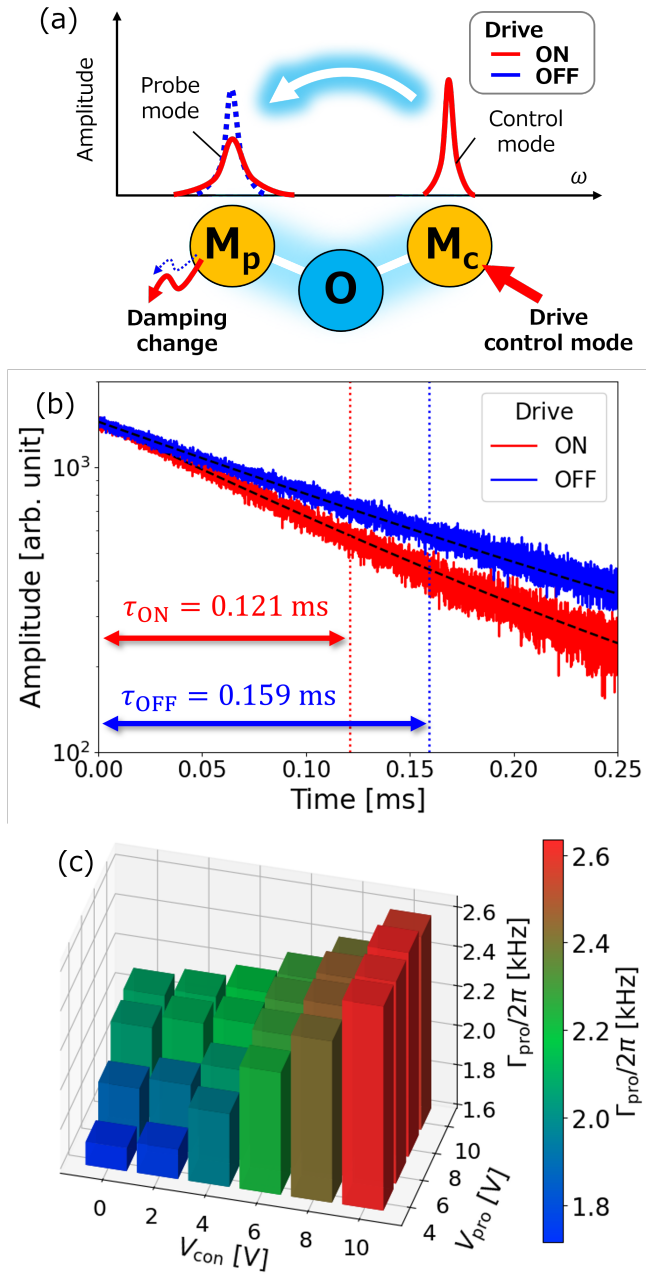


FIG. 4. (a) Concept of cross-nonlinear damping in a multi-mode optomechanical system, where a single optical mode (O) is coupled to two mechanical modes: a probe mode ( $M_p$ ) and a control mode ( $M_c$ ). The probe and control modes were resonantly driven at frequencies  $f_{pro} = 48.0$  MHz and  $f_{con} = 48.5$  MHz, respectively. (b) Ring-down measurements of the probe mode with the control mode strongly driven (ON, red) or un-driven (OFF, blue) showing an approximate 0.6 kHz increase in damping. The data were obtained with drive voltages  $V_{pro} = 6.0$  V and  $V_{con} = 10.0$  V, where  $V_{pro}$  and  $V_{con}$  denote the drive voltages for the probe and control modes, respectively. (c) Increase in probe-mode damping rate  $\Gamma_{pro}/2\pi$  as a function of drive voltages reveals both self-nonlinear damping (dependence on  $V_{pro}$ ) and cross-nonlinear damping (dependence on  $V_{con}$ ). The damping rates are extracted from linear fits to the ring-down traces.

# Supplemental Material for “Optically tunable nonlinear mechanical damping in an optomechanical resonator”

Hideki Arahari, Motoki Asano, Hiroshi Yamaguchi, Hajime Okamoto

Basic Research Laboratories, NTT, Inc., 3-1 Morinosato Wakamiya, Atsugi-shi, Kanagawa 243-0198 Japan

## MEMORY EFFECTS IN NONLINEAR OPTOMECHANICAL COUPLING

We consider a single optical cavity mode that is simultaneously coupled via radiation pressure to multiple mechanical modes. The equations of motion for this optomechanical system are

$$\dot{a}(t) = \left[ i\Delta - \frac{\kappa_{\text{cav}}}{2} \right] a(t) + i \sum_j g_j q_j(t) a(t) + \sqrt{\kappa_{\text{in}}} a_{\text{in}}(t), \quad (\text{S1})$$

$$\ddot{q}_j(t) + \Gamma_j \dot{q}_j(t) + \Omega_j^2 q_j(t) = 2g_j \Omega_j |a(t)|^2. \quad (\text{S2})$$

Here,  $a(t)$  denotes the amplitude of the intracavity optical mode driven by input field  $a_{\text{in}}(t)$ . The laser detuning is defined as  $\Delta = \omega_L - \omega_{\text{cav}}$ , where  $\omega_L$  is the angular frequency of the input laser and  $\omega_{\text{cav}}$  is the cavity resonance frequency. Parameter  $\kappa_{\text{cav}}$  is the total cavity decay rate with external coupling rate  $\kappa_{\text{in}}$ . The mechanical displacement normalized by zero-point fluctuation amplitude,  $q_j(t) (\equiv x_j / x_{\text{zpf},j})$ , has resonance frequency  $\Omega_j$ , damping rate  $\Gamma_j$ , and effective mass  $m_{\text{eff},j}$ . Linearized optomechanical coupling strength  $G_j$  and single-photon optomechanical coupling strength  $g_j$  are given by  $G_j = \partial \omega_{\text{cav}} / \partial x_j$  and  $g_j = G_j x_{\text{zpf},j}$ , respectively. The zero-point fluctuation amplitude is  $x_{\text{zpf},j} = \sqrt{\hbar / (2m_{\text{eff},j} \Omega_j)}$ . In the following, we assume a continuous-wave drive, so  $a_{\text{in}}(t) = a_{\text{in}} = \text{const}$ . In addition, we introduce rotating-frame transformation  $a(t) = \tilde{a}(t) e^{(i\Delta - \frac{\kappa_{\text{cav}}}{2})t} = \tilde{a}(t) e^{\lambda_0 t}$ , which factorizes out the fast time-evolution of the photon mode

$$\dot{\tilde{a}}(t) = i \sum_j g_j q_j(t) \tilde{a}(t) + \sqrt{\kappa_{\text{in}}} a_{\text{in}} e^{-\lambda_0 t}, \quad (\text{S3})$$

where we introduce  $\lambda_0 = i\Delta - \kappa_{\text{cav}}/2$  to simply express the equations.

To introduce a description that explicitly accounts for the delayed optical response with respect to the mechanical motion, we treat the photon mode using a formal integral solution that incorporates the history (memory) of the mechanical displacement. Integrating this equation from  $s = -\infty$  to  $t$ , we obtain

$$\begin{aligned} \tilde{a}(t) &= \int_{-\infty}^t \dot{\tilde{a}}(s) ds = \sqrt{\kappa_{\text{in}}} a_{\text{in}} \int_{-\infty}^t e^{-\lambda_0 s} ds + i \sum_j g_j \int_{-\infty}^t q_j(s) \tilde{a}(s) ds \\ &= \sqrt{\kappa_{\text{in}}} a_{\text{in}} \chi_0(\Delta) e^{-\lambda_0 t} + i \sum_j g_j \int_{-\infty}^t q_j(s) \tilde{a}(s) ds, \end{aligned} \quad (\text{S4})$$

where the susceptibility is  $\chi_0(\Delta) = (\kappa_{\text{cav}}/2 - i\Delta)^{-1}$ . The right-hand side of Eq. (S4) again depends on  $\tilde{a}$ . By recursively substituting the formal solution into the right-hand side, higher-order terms are generated. These recursively generated terms give rise to the nonlinear optomechanical coupling. Expanding in powers of  $g_j$  yields the first-order optomechanical coupling and higher-order contributions. Substituting the formal solution again into the higher-order term and truncating at the third order in  $g_j$ , we obtain

$$\begin{aligned} \tilde{a}(t) &\approx \sqrt{\kappa_{\text{in}}} a_{\text{in}} \chi_0(\Delta) e^{-\lambda_0 t} + i \sqrt{\kappa_{\text{in}}} a_{\text{in}} \chi_0(\Delta) \sum_j g_j \int_{-\infty}^t q_j(s) e^{-\lambda_0 s} ds \\ &\quad + i^2 \sqrt{\kappa_{\text{in}}} a_{\text{in}} \chi_0(\Delta) \sum_{j,k} g_j g_k \int_{-\infty}^t \int_{-\infty}^s q_j(s) q_k(s') e^{-\lambda_0 s'} ds ds' \\ &\quad + i^3 \sqrt{\kappa_{\text{in}}} a_{\text{in}} \chi_0(\Delta) \sum_{j,k,l} g_j g_k g_l \int_{-\infty}^t \int_{-\infty}^s \int_{-\infty}^{s'} q_j(s) q_k(s') q_l(s'') e^{-\lambda_0 s''} ds ds' ds''. \end{aligned} \quad (\text{S5})$$

In the final expression, the third and fourth terms on the right-hand side correspond to the second- and third-order nonlinear optomechanical coupling terms, respectively.

If we restrict the analysis to linear (first-order) optomechanical coupling, the terms beyond the second line of Eq. (S5) can be ignored. Introducing a change in variables,  $s = t - \tau$  with  $\tau \geq 0$ , the integral in the second term,  $J_1^{(j)}(t)$ , becomes

$$J_1^{(j)}(t) = \int_{-\infty}^t q_j(s) e^{-\lambda_0 s} ds = e^{-\lambda_0 t} \int_0^\infty K^{(1)}(\tau) q_j(t - \tau) d\tau, \quad (\text{S6})$$

where

$$\lambda_0 = i\Delta - \kappa_{\text{cav}}/2, \quad K^{(1)}(\tau) = e^{\lambda_0 \tau}. \quad (\text{S7})$$

Here  $K^{(1)}(\tau)$  represents the first-order memory kernel, and Eq. (S6) can be interpreted as a memory integral over delay time  $\tau$ . This representation allows us to incorporate explicitly how the past mechanical displacement,  $q_j(t - \tau)$ , contributes to the present optical response.

In an analogous way, we can introduce memory kernels for the second- and third-order optomechanical coupling terms. For the double integral (third term in Eq. (S5)) we define  $J_2^{(j,k)}(t)$  as

$$J_2^{(j,k)}(t) = \int_{-\infty}^t q_j(s) \int_{-\infty}^s q_k(s') e^{-\lambda_0 s'} ds' ds, \quad (\text{S8})$$

where  $\lambda_0 \equiv i\Delta - \kappa_{\text{cav}}/2$ . Introducing time differences  $\tau_1 = t - s$  and  $\tau_2 = s - s'$ , *i.e.*,  $s = t - \tau_1$  and  $s' = t - \tau_1 - \tau_2$ , and noting that  $\tau_1 \geq 0$  and  $\tau_2 \geq 0$ , the integral can be rewritten as

$$J_2^{(j,k)}(t) = e^{-\lambda_0 t} \int_0^\infty \int_0^\infty K^{(2)}(\tau_1, \tau_2) \mathcal{X}_{j,k}(\tau_1, \tau_2) d\tau_1 d\tau_2, \quad (\text{S9})$$

$$\mathcal{X}_{j,k}(\tau_1, \tau_2) = q_j(t - \tau_1) q_k(t - \tau_1 - \tau_2), \quad (\text{S10})$$

$$K^{(2)}(\tau_1, \tau_2) = e^{\lambda_0 \tau_1} e^{\lambda_0 \tau_2}. \quad (\text{S11})$$

This is referred to as the second-order memory integral.

Finally, triple integral  $J_3^{(j,k,l)}(t)$ , which corresponds to the integral part of the fourth term in Eq. (S5), can be written as

$$J_3^{(j,k,l)}(t) = \int_{-\infty}^t q_j(s) \int_{-\infty}^s q_k(s') \int_{-\infty}^{s'} q_l(s'') e^{-\lambda_0 s''} ds'' ds' ds. \quad (\text{S12})$$

Introducing time differences  $\tau_1 = t - s$ ,  $\tau_2 = s - s'$ , and  $\tau_3 = s' - s''$ , *i.e.*,  $s = t - \tau_1$ ,  $s' = t - \tau_1 - \tau_2$ , and  $s'' = t - \tau_1 - \tau_2 - \tau_3$ , and using  $\tau_1, \tau_2, \tau_3 \geq 0$ , we obtain the following.

$$J_3^{(j,k,l)}(t) = e^{-\lambda_0 t} \int_0^\infty \int_0^\infty \int_0^\infty K^{(3)}(\tau_1, \tau_2, \tau_3) \mathcal{X}_{j,k,l}(\tau_1, \tau_2, \tau_3) d\tau_1 d\tau_2 d\tau_3 \quad (\text{S13})$$

$$\mathcal{X}_{j,k,l}(\tau_1, \tau_2, \tau_3) = q_j(t - \tau_1) q_k(t - \tau_1 - \tau_2) q_l(t - \tau_1 - \tau_2 - \tau_3), \quad (\text{S14})$$

$$K^{(3)}(\tau_1, \tau_2, \tau_3) = e^{\lambda_0 \tau_1} e^{\lambda_0 \tau_2} e^{\lambda_0 \tau_3}, \quad (\text{S15})$$

where  $K^{(3)}$  is the third-order memory kernel. Using the definitions of the first-, second-, and third-order optomechanical memory integrals in Eqs. (S6) - (S13), the solution of the photon-field in Eq. (S5), which was transformed back from the rotating frame, can be compactly rewritten as

$$a(t) = \sqrt{\kappa_{\text{in}} a_{\text{in}} \chi_0(\Delta)} \left( 1 + i \sum_j g_j J_1^{(j)}(t) e^{\lambda_0 t} + i^2 \sum_{j,k} g_j g_k J_2^{(j,k)}(t) e^{\lambda_0 t} + i^3 \sum_{j,k,l} g_j g_k g_l J_3^{(j,k,l)}(t) e^{\lambda_0 t} \right). \quad (\text{S16})$$

Next, we also expand the equation of motion for the mechanical displacement. In the parameter regime of interest,  $\kappa_{\text{cav}} \sim \Omega_j$  (partly resolved sideband regime), the optomechanical interaction is in the non-adiabatic regime such that the mechanical resonance frequency appears as sidebands in the optical response. Mechanical displacement  $q_j(t)$  is treated as a single-frequency oscillation at  $\Omega_j$  with slowly varying complex amplitude  $B_j(t)$  and can be written as

$$q_j(t) = B_j(t) e^{-i\Omega_j t} + \text{c.c.} \quad (\text{S17})$$

Then  $\dot{q}_j(t)$  and  $\ddot{q}_j(t)$  are, respectively, given by

$$\begin{aligned}\dot{q}_j(t) &= \left( \dot{B}_j - i\Omega_j B_j \right) e^{-i\Omega_j t} + \text{c.c.}, \\ \ddot{q}_j(t) &= \left( \ddot{B}_j - 2i\Omega_j \dot{B}_j - \Omega_j^2 B_j \right) e^{-i\Omega_j t} + \text{c.c.}\end{aligned}\quad (\text{S18})$$

Collecting terms proportional to  $e^{-i\Omega_j t}$ , we obtain the exact equations of motion for complex amplitudes

$$-2i\Omega_j \dot{B}_j - \Omega_j^2 B_j + \Gamma_j \left( \dot{B}_j - i\Omega_j B_j \right) + \Omega_j^2 B_j(t) = 2g_j \Omega_j |a(t)|^2. \quad (\text{S19})$$

Assuming that the envelope varies slowly compared to the mechanical oscillation,  $|\dot{B}_j| \ll \Omega_j |B_j|$  and  $|\ddot{B}_j| \ll \Omega_j |\dot{B}_j|$ , we ignore  $\ddot{B}_j$  and  $\Gamma_j \dot{B}_j$  compared with  $\Omega_j \dot{B}_j$ . Then the equation of motion for  $B_j$  reduces to

$$\begin{aligned}-2i\Omega_j \dot{B}_j - i\Gamma_j \Omega_j B_j(t) &\approx 2g_j \Omega_j |a(t)|^2 \\ \Rightarrow \dot{B}_j(t) &= -\frac{\Gamma_j}{2} B_j(t) + ig_j |a(t)|^2.\end{aligned}\quad (\text{S20})$$

The envelope equation for mode  $j$  can be rewritten by introducing complex oscillation amplitude  $b_j(t) = B_j(t) e^{-i\Omega_j t}$  as

$$\dot{b}_j(t) = -i\Omega_j b_j(t) - \frac{\Gamma_j}{2} b_j(t) + ig_j |a(t)|^2. \quad (\text{S21})$$

We next apply the same procedure to a nonlinear mechanical oscillator with Duffing and nonlinear damping terms, transforming its equation of motion into one for slowly varying envelope  $B_j(t)$

$$\ddot{q}_j + \left( \Omega_j^2 + \sum_i \alpha_{ij} x_{\text{zpf},i}^2 q_i^2 \right) q_j + \left( \Gamma_j + \sum_i \beta_{ij} x_{\text{zpf},i}^2 q_i^2 \right) \dot{q}_j = 2g_j \Omega_j |a(t)|^2. \quad (\text{S22})$$

Here,  $\alpha_{ij}$  and  $\beta_{ij}$  denote the Duffing and nonlinear-damping coefficients, respectively. The terms with  $i = j$  represent self-nonlinearity, while those with  $i \neq j$  correspond to cross-nonlinearity arising from other mechanical modes. The Duffing term can be expanded as

$$\begin{aligned}q_i^2 q_j &= \left( B_i^2 e^{-2i\Omega_i t} + 2|B_i|^2 + B_i^{*2} e^{2i\Omega_i t} \right) (B_j e^{-i\Omega_j t} + \text{c.c.}) \\ &= B_i^2 B_j e^{-2i\Omega_i t} e^{-i\Omega_j t} + 2|B_i|^2 B_j e^{-i\Omega_j t} + B_i^{*2} B_j e^{2i\Omega_i t} e^{-i\Omega_j t} + \text{c.c.}\end{aligned}\quad (\text{S23})$$

When the two mechanical frequencies are nearly equal

$$|\Omega_i - \Omega_j|/\Omega_i \ll 1, \quad |\Omega_i - \Omega_j|/\Omega_j \ll 1 \quad (\text{S24})$$

the slowly varying (positive-frequency) component relevant to self- and cross-Duffing interactions reduces to

$$q_i^2 q_j|_+ \approx 3|B_i|^2 B_j e^{-i\Omega_j t}. \quad (\text{S25})$$

For the nonlinear damping term, we have

$$q_i^2 \dot{q}_j = \left( B_i^2 e^{-2i\Omega_i t} + 2|B_i|^2 + B_i^{*2} e^{2i\Omega_i t} \right) \left[ \left( \dot{B}_j - i\Omega_j B_j \right) e^{-i\Omega_j t} + \text{c.c.} \right]. \quad (\text{S26})$$

Extracting the positive-frequency component yields

$$q_i^2 \dot{q}_j|_+ = 2|B_i|^2 \left( \dot{B}_j - i\Omega_j B_j \right) e^{-i\Omega_j t} + B_i^2 e^{-2i\Omega_i t} \left( \dot{B}_j^* + i\Omega_j B_j^* \right) e^{i\Omega_j t}. \quad (\text{S27})$$

Under the same near-degeneracy condition as Duffing terms

$$|\Omega_i - \Omega_j|/\Omega_i \ll 1, \quad |\Omega_i - \Omega_j|/\Omega_j \ll 1 \quad (\text{S28})$$

dominant slowly varying component ( $|\dot{B}_j| \ll \Omega_j |B_j|$ ) becomes

$$q_i^2 \dot{q}_j|_+ \approx -i\Omega_j |B_i|^2 B_j e^{-i\Omega_j t}. \quad (\text{S29})$$

Since the system satisfies the near-degenerate condition for the mechanical frequencies, the nonlinear envelope equation for mode  $j$  can be rewritten by introducing complex oscillation amplitude  $b_j(t) = B_j(t)e^{-i\Omega_j t}$  as

$$\begin{aligned} \dot{b}_j = & - \left( \frac{\Gamma_j}{2} + \sum_i \frac{\beta_{ij}}{2} x_{\text{zpf},i}^2 |b_i|^2 \right) b_j - i \left( \Omega_j + \sum_i \frac{3}{2\Omega_j} \alpha_{ij} x_{\text{zpf},i}^2 |b_i|^2 \right) b_j \\ & + i g_j |a(t)|^2 e^{-i\Omega_m t}. \end{aligned} \quad (\text{S30})$$

## OPTICALLY INDUCED MECHANICAL NONLINEARITY IN A SINGLE MECHANICAL MODE

For clarity, we first analyze the case of a single mechanical mode and derive the higher-order optomechanical interaction terms analytically, thereby demonstrating how optical fields induce mechanical nonlinearities. To focus on a single mechanical oscillator, we rewrite the notation used in the previous section as

$$m_{\text{eff},j} \rightarrow m_{\text{eff}}, \quad q_j \rightarrow q, \quad \Omega_j \rightarrow \Omega_m, \quad \Gamma_j \rightarrow \Gamma_m, \quad B_j \rightarrow B, \quad b_j \rightarrow b \quad (\text{S31})$$

and similarly remove mode indices from other related quantities so that no confusion arises.

### First-order optomechanical coupling

We now focus on the first-order optomechanical coupling. If the optical response has no delay, *i.e.*,  $K^{(1)}(\tau)$  does not depend on time, the kernel reduces to delta function  $K^{(1)}(\tau) = \delta(\tau)$  and the integral yields

$$\int_0^\infty K^{(1)}(\tau)q(t-\tau)d\tau = q(t). \quad (\text{S32})$$

In this case,  $\tau = 0$  and there is no response delay in the optomechanical coupling. Such a situation corresponds to the bad-cavity limit ( $\kappa_{\text{cav}} \gg \Omega_m$ , adiabatic regime), where the optical mode responds instantaneously compared to the mechanical motion. In the following, we are interested in memory effects where the past mechanical motion influences the future optical response.

Substituting the single-mode ansatz of Eq. (S17) into Eq. (S6) and assuming that  $B(t)$  vary slowly on the mechanical timescale ( $B(t-\tau) \simeq B(t)$ ), we obtain

$$\begin{aligned} J_1(t)e^{\lambda_0 t} &= \int_0^\infty K^{(1)}(\tau)q(t-\tau)d\tau \simeq \int_0^\infty K^{(1)}(\tau) \left( B(t)e^{-i\Omega_m(t-\tau)} + \text{c.c.} \right) d\tau \\ &= B(t)e^{-i\Omega_m t} \int_0^\infty K^{(1)}(\tau)e^{i\Omega_m \tau} d\tau + B^*(t)e^{i\Omega_m t} \int_0^\infty K^{(1)}(\tau)e^{-i\Omega_m \tau} d\tau \\ &= \chi_+^{(1)}b(t) + \chi_-^{(1)}b^*(t), \end{aligned} \quad (\text{S33})$$

where the memory integrals can be evaluated as

$$\int_0^\infty K^{(1)}e^{\pm i\Omega_m \tau} d\tau = \int_0^\infty e^{(i(\Delta \pm \Omega_m) - \kappa_{\text{cav}}/2)\tau} d\tau = \left[ \frac{e^{\lambda_\pm \tau}}{\lambda_\pm} \right]_0^\infty = \frac{1}{(-\lambda_\pm)} \equiv \chi_\pm^{(1)}, \quad (\text{S34})$$

with  $\lambda_\pm = i(\Delta \pm \Omega_m) - \kappa_{\text{cav}}/2$ . Thus the integral yields the first-order susceptibility of the optomechanical coupling. In the following, we denote these susceptibilities by  $\chi_\pm^{(1)}$ .

### Second-order optomechanical coupling

We next evaluate the second-order optomechanical coupling term. Substituting the single-mode ansatz of Eq. (S17) into Eq. (S9) and again assuming that  $B(t - \tau) \simeq B(t)$ , we obtain

$$\begin{aligned}
J_2(t)e^{\lambda t} &= \int_0^\infty \int_0^\infty K^{(2)}(\tau_1, \tau_2) q(t - \tau_1) q(t - \tau_1 - \tau_2) d\tau_1 d\tau_2 \\
&\simeq \int_0^\infty \int_0^\infty K^{(2)}(\tau_1, \tau_2) \left( B(t)e^{-i\Omega_m(t-\tau_1)} + \text{c.c.} \right) \left( B(t)e^{-i\Omega_m(t-\tau_1-\tau_2)} + \text{c.c.} \right) d\tau_1 d\tau_2 \\
&= B^2(t)e^{-2i\Omega_m t} \int_0^\infty \int_0^\infty K^{(2)}(\tau_1, \tau_2) e^{2i\Omega_m \tau_1} e^{i\Omega_m \tau_2} d\tau_1 d\tau_2 \\
&\quad + B(t)B^*(t) \int_0^\infty \int_0^\infty K^{(2)}(\tau_1, \tau_2) (e^{-i\Omega_m \tau_2} + e^{i\Omega_m \tau_2}) d\tau_1 d\tau_2 \\
&\quad + B^{*2}(t)e^{2i\Omega_m t} \int_0^\infty \int_0^\infty K^{(2)}(\tau_1, \tau_2) e^{-2i\Omega_m \tau_1} e^{-i\Omega_m \tau_2} d\tau_1 d\tau_2 \\
&= \chi_{+2}^{(1)} \chi_{+}^{(1)} B^2(t)e^{-2i\Omega_m t} + \chi_0^{(1)} (\chi_{-}^{(1)} + \chi_{+}^{(1)}) B(t)B^*(t) + \chi_{-2}^{(1)} \chi_{-}^{(1)} B^{*2}(t)e^{2i\Omega_m t}, \tag{S35}
\end{aligned}$$

$$= \chi_{+2}^{(1)} \chi_{+}^{(1)} b^2(t) + \chi_0^{(1)} (\chi_{-}^{(1)} + \chi_{+}^{(1)}) b(t)b^*(t) + \chi_{-2}^{(1)} \chi_{-}^{(1)} b^{*2}(t), \tag{S36}$$

where we use  $\lambda_{\pm n} = \lambda \pm in\Omega_m = i(\Delta \pm n\Omega_m) - \kappa_{\text{cav}}/2$  and

$$\begin{aligned}
\int_0^\infty \int_0^\infty K^{(2)} e^{\pm ni\Omega_m \tau_1} e^{\pm mi\Omega_m \tau_2} d\tau_1 d\tau_2 &= \int_0^\infty \int_0^\infty e^{(\lambda \pm ni\Omega_m)\tau_1} e^{(\lambda \pm mi\Omega_m)\tau_2} d\tau_1 d\tau_2 \\
&= \left[ \frac{e^{(\lambda \pm ni\Omega_m)\tau_1}}{\lambda \pm ni\Omega_m} \right]_0^\infty \left[ \frac{e^{(\lambda \pm mi\Omega_m)\tau_2}}{\lambda \pm mi\Omega_m} \right]_0^\infty \\
&= \frac{1}{(-\lambda_{\pm n})} \frac{1}{(-\lambda_{\pm m})} \equiv \chi_{\pm n}^{(1)} \chi_{\pm m}^{(1)}. \tag{S37}
\end{aligned}$$

Here we expressed the result in terms of first-order optomechanical susceptibilities  $\chi^{(1)}$ , and  $\chi_0^{(1)} = (-\lambda_0)^{-1} = (\kappa_{\text{cav}}/2 - i\Delta)^{-1}$ .

### Third-order optomechanical coupling

Finally, we consider the third-order optomechanical coupling term. Substituting the single-mode ansatz of Eq. (S17) into Eq. (S13) and again using  $B(t - \tau) \simeq B(t)$ , we obtain

$$\begin{aligned}
J_3(t)e^{\lambda t} &= \int_0^\infty \int_0^\infty \int_0^\infty K^{(3)}(\tau_1, \tau_2, \tau_3) q(t - \tau_1) q(t - \tau_1 - \tau_2) q(t - \tau_1 - \tau_2 - \tau_3) d\tau_1 d\tau_2 d\tau_3 \\
&\simeq \int_0^\infty \int_0^\infty \int_0^\infty K^{(3)}(\tau_1, \tau_2, \tau_3) \\
&\quad \left( B(t)e^{-i\Omega_m(t-\tau_1)} + \text{c.c.} \right) \left( B(t)e^{-i\Omega_m(t-\tau_1-\tau_2)} + \text{c.c.} \right) \left( B(t)e^{-i\Omega_m(t-\tau_1-\tau_2-\tau_3)} + \text{c.c.} \right) d\tau_1 d\tau_2 d\tau_3 \\
&= B^3(t)e^{-3i\Omega_m t} \int_0^\infty \int_0^\infty \int_0^\infty K^{(3)}(\tau_1, \tau_2, \tau_3) e^{3i\Omega_m \tau_1} e^{2i\Omega_m \tau_2} e^{i\Omega_m \tau_3} d\tau_1 d\tau_2 d\tau_3 \\
&\quad + B^2(t)B^*(t)e^{-i\Omega_m t} \\
&\quad \int_0^\infty \int_0^\infty \int_0^\infty K^{(3)}(\tau_1, \tau_2, \tau_3) \left( e^{i\Omega_m \tau_1} e^{-i\Omega_m \tau_3} + e^{i\Omega_m \tau_1} e^{i\Omega_m \tau_3} + e^{i\Omega_m \tau_1} e^{2i\Omega_m \tau_2} e^{i\Omega_m \tau_3} \right) d\tau_1 d\tau_2 d\tau_3 \\
&\quad + B(t)B^{*2}(t)e^{i\Omega_m t} \\
&\quad \int_0^\infty \int_0^\infty \int_0^\infty K^{(3)}(\tau_1, \tau_2, \tau_3) \left( e^{-i\Omega_m \tau_1} e^{-2i\Omega_m \tau_2} e^{-i\Omega_m \tau_3} + e^{-i\Omega_m \tau_1} e^{-i\Omega_m \tau_3} + e^{-i\Omega_m \tau_1} e^{i\Omega_m \tau_3} \right) d\tau_1 d\tau_2 d\tau_3 \\
&\quad + B^{*3}(t)e^{3i\Omega_m t} \int_0^\infty \int_0^\infty \int_0^\infty K^{(3)}(\tau_1, \tau_2, \tau_3) e^{-3i\Omega_m \tau_1} e^{-2i\Omega_m \tau_2} e^{-i\Omega_m \tau_3} d\tau_1 d\tau_2 d\tau_3 \\
&= \chi_{+3}^{(1)} \chi_{+2}^{(1)} \chi_{+}^{(1)} B^3(t) e^{-3i\Omega_m t} + \left( \chi_{+}^{(1)} \chi_0^{(1)} \chi_{-}^{(1)} + \left( \chi_{+}^{(1)} \right)^2 \chi_0^{(1)} + \left( \chi_{+}^{(1)} \right)^2 \chi_{+2}^{(1)} \right) B^2(t) B^*(t) e^{-i\Omega_m t} \\
&\quad + \left( \left( \chi_{-}^{(1)} \right)^2 \chi_{-2}^{(1)} + \left( \chi_{-}^{(1)} \right)^2 \chi_0^{(1)} + \chi_{-}^{(1)} \chi_0^{(1)} \chi_{+}^{(1)} \right) B(t) B^{*2}(t) e^{i\Omega_m t} + \chi_{-3}^{(1)} \chi_{-2}^{(1)} \chi_{-}^{(1)} B^{*3}(t) e^{3i\Omega_m t}, \\
&= \chi_{+3}^{(1)} \chi_{+2}^{(1)} \chi_{+}^{(1)} b^3(t) + \left( \chi_{+}^{(1)} \chi_0^{(1)} \chi_{-}^{(1)} + \left( \chi_{+}^{(1)} \right)^2 \chi_0^{(1)} + \left( \chi_{+}^{(1)} \right)^2 \chi_{+2}^{(1)} \right) |b(t)|b(t) \\
&\quad + \left( \left( \chi_{-}^{(1)} \right)^2 \chi_{-2}^{(1)} + \left( \chi_{-}^{(1)} \right)^2 \chi_0^{(1)} + \chi_{-}^{(1)} \chi_0^{(1)} \chi_{+}^{(1)} \right) |b(t)|b^*(t) + \chi_{-3}^{(1)} \chi_{-2}^{(1)} \chi_{-}^{(1)} b^{*3}(t), \tag{S38}
\end{aligned}$$

where the integrals have been evaluated using

$$\begin{aligned}
&\int \int \int_0^\infty K^{(3)} e^{\pm li\Omega_m \tau_1} e^{\pm mi\Omega_m \tau_2} e^{\pm ni\Omega_m \tau_3} d\tau_1 d\tau_2 d\tau_3 \\
&= \int \int \int_0^\infty e^{(\lambda \pm li\Omega_m) \tau_1} e^{(\lambda \pm mi\Omega_m) \tau_2} e^{(\lambda \pm ni\Omega_m) \tau_3} d\tau_1 d\tau_2 d\tau_3 \\
&= \left[ \frac{e^{(\lambda \pm li\Omega_m) \tau_1}}{\lambda \pm li\Omega_m} \right]_0^\infty \left[ \frac{e^{(\lambda \pm mi\Omega_m) \tau_2}}{\lambda \pm mi\Omega_m} \right]_0^\infty \left[ \frac{e^{(\lambda \pm ni\Omega_m) \tau_3}}{\lambda \pm ni\Omega_m} \right]_0^\infty \\
&= \frac{1}{(-\lambda \pm l)} \frac{1}{(-\lambda \pm m)} \frac{1}{(-\lambda \pm n)} \equiv \chi_{\pm l}^{(1)} \chi_{\pm m}^{(1)} \chi_{\pm n}^{(1)}, \tag{S39}
\end{aligned}$$

expressed in terms of first-order susceptibilities  $\chi^{(1)}$ .

### Mechanical nonlinearity induced by radiation pressure

We now summarize the above to derive the contribution of radiation pressure to the effective mechanical nonlinearity. The photon mode including nonlinear optomechanical coupling [Eq. (S5)] can be formally written as

$$\tilde{a}(t) = \sqrt{\kappa_{\text{in}}} a_{\text{in}} \chi_0(\Delta) \left( e^{-\lambda_0 t} + \sum_n (ig_0)^n J_n(t) \right). \quad (\text{S40})$$

Here we restrict ourselves to terms up to the third order in  $G$ . Using Eqs. (S33), (S36), and (S38), the solution, which is transformed back from the rotating frame, can be written as

$$a(t) = \sqrt{\kappa_{\text{in}}} a_{\text{in}} \chi_0(\Delta) (1 + ig_0 J_1(t) e^{\lambda_0 t} + (ig_0)^2 J_2(t) e^{\lambda_0 t} + (ig_0)^3 J_3(t) e^{\lambda_0 t}). \quad (\text{S41})$$

Using the intracavity photon number in the absence of optomechanical backaction,  $n_{\text{cav}}(\Delta) = \kappa_{\text{in}} |a_{\text{in}}|^2 |\chi_0(\Delta)|^2$ , the intracavity intensity can then be written as

$$|a(t)|^2 = n_{\text{cav}}(\Delta) |1 + ig_0 J_1(t) e^{\lambda_0 t} + (ig_0)^2 J_2(t) e^{\lambda_0 t} + (ig_0)^3 J_3(t) e^{\lambda_0 t}|^2. \quad (\text{S42})$$

We define

$$E(t) = 1 + ig_0 \mathcal{A} + (ig_0)^2 \mathcal{B} + (ig_0)^3 \mathcal{C} \quad (\text{S43})$$

$$\text{where } \mathcal{A}(t) = J_1(t) e^{\lambda_0 t}, \quad \mathcal{B}(t) = J_2(t) e^{\lambda_0 t}, \quad \mathcal{C}(t) = J_3(t) e^{\lambda_0 t}, \quad (\text{S44})$$

and expand  $|E(t)|^2$  using

$$E = 1 + ig_0 \mathcal{A} + (ig_0)^2 \mathcal{B} + (ig_0)^3 \mathcal{C}, \quad E^* = 1 - ig_0 \mathcal{A}^* + (-ig_0)^2 \mathcal{B}^* + (-ig_0)^3 \mathcal{C}^*. \quad (\text{S45})$$

When expanding  $|E(t)|^2$ , the components at frequencies  $\pm\Omega_m$  in products  $J_1[\pm\Omega_m]$ ,  $J_2[\pm 2\Omega_m, 0\Omega_m]$ , and  $J_3[\pm\Omega_m, \pm 3\Omega_m]$  yield contributions  $F_{\pm}$  to the radiation pressure force. Focusing on positively rotating component  $F_+[+\Omega_m]$ , the relevant terms are

$$J_1[+\Omega_m], \quad (J_1[-\Omega_m])^*, \quad (\text{S46})$$

$$J_3[+\Omega_m], \quad (J_3[-\Omega_m])^*, \quad (\text{S47})$$

$$J_1[-\Omega_m] (J_2[-2\Omega_m])^*, \quad (J_1[+\Omega_m])^* J_2[+2\Omega_m], \\ J_1[+\Omega_m] (J_2[0\Omega_m])^*, \quad (J_1[-\Omega_m])^* J_2[0\Omega_m], \quad (\text{S48})$$

$$J_2[0\Omega_m] (J_3[-\Omega_m])^*, \quad (J_2[0\Omega_m])^* J_3[+\Omega_m], \\ J_3[+3\Omega_m] (J_2[+2\Omega_m])^*, \quad (J_3[-3\Omega_m])^* J_2[-2\Omega_m], \quad (\text{S49})$$

i.e., twelve terms in total. Since the higher-order terms in  $g_0$  (above the fourth order in intensity) are relatively smaller than the other terms, we ignore them and retain only the eight terms in Eqs. (S46)–(S48). Note that  $\chi_{\pm}^{(1)*} \neq \chi_{\mp}^{(1)}$  in general, so  $|E(t)|^2$  can be written as

$$\begin{aligned} |E(t)|^2 &\simeq \left( ig_0 J_1[+\Omega_m] - ig_0 (J_1[-\Omega_m])^* + (ig_0)^3 J_3[+\Omega_m] + \left( (ig_0)^3 J_3[-\Omega_m] \right)^* \right. \\ &\quad \left. + (ig_0)^3 J_1[-\Omega_m] (J_2[-2\Omega_m])^* - (ig_0)^3 (J_1[+\Omega_m])^* J_2[+2\Omega_m] \right. \\ &\quad \left. + (ig_0)^3 J_1[+\Omega_m] (J_2[0\Omega_m])^* - (ig_0)^3 (J_1[-\Omega_m])^* J_2[0\Omega_m] \right) \\ &= ig_0 \left( \chi_+^{(1)} - \chi_-^{(1)*} \right) B(t) \\ &\quad + (ig_0)^3 \left\{ \left( \chi_+^{(1)} \chi_0^{(1)} \chi_-^{(1)} + \left( \chi_+^{(1)} \right)^2 \chi_0^{(1)} + \left( \chi_+^{(1)} \right)^2 \chi_{+2}^{(1)} \right) \right. \\ &\quad \left. - \left( \chi_-^{(1)} \chi_0^{(1)} \chi_+^{(1)} + \left( \chi_-^{(1)} \right)^2 \chi_0^{(1)} + \left( \chi_-^{(1)} \right)^2 \chi_{-2}^{(1)} \right)^* \right\} |B|^2 B(t) \end{aligned} \quad (\text{S50})$$

$$\begin{aligned} &\quad + (ig_0)^3 \left( \chi_-^{(1)} \chi_{-2}^{(1)*} \chi_-^{(1)*} - \chi_+^{(1)*} \chi_{+2}^{(1)} \chi_+^{(1)} \right) |B|^2 B(t) \\ &\quad + (ig_0)^3 \left\{ \chi_+^{(1)} \chi_0^{(1)*} \left( \chi_+^{(1)} + \chi_-^{(1)} \right)^* - \chi_-^{(1)*} \chi_0^{(1)} \left( \chi_-^{(1)} + \chi_+^{(1)} \right) \right\} |B|^2 B(t) \end{aligned} \quad (\text{S51})$$

$$= -g_0 C_1(\Delta) B(t) - g_0^3 (C_2(\Delta) + C_3(\Delta) + C_4(\Delta)) |B|^2 B(t), \quad (\text{S52})$$

where we introduce linear contribution  $C_1$  and nonlinear contributions  $C_2$ ,  $C_3$ , and  $C_4$ , respectively, as

$$C_1(\Delta) = -i \left( \chi_+^{(1)} - \chi_-^{(1)*} \right) = \frac{1}{(\Delta + \Omega_m) + i\kappa_{\text{cav}}/2} + \frac{1}{(\Delta - \Omega_m) - i\kappa_{\text{cav}}/2}, \quad (\text{S53})$$

$$C_{2,3,4}(\Delta) = i [S_{2,3,4}^+ - (S_{2,3,4}^-)^*], \quad (\text{S54})$$

$$S_2^\pm = \chi_\pm^{(1)} \chi_0^{(1)} \chi_\mp^{(1)} + \left( \chi_\pm^{(1)} \right)^2 \chi_0^{(1)} + \left( \chi_\pm^{(1)} \right)^2 \chi_{\pm 2}^{(1)}, \quad (\text{S55})$$

$$S_3^\pm = \chi_\mp^{(1)} \chi_{\mp 2}^{(1)*} \chi_\mp^{(1)*}, \quad (\text{S56})$$

$$S_4^\pm = \chi_\pm^{(1)} \chi_0^{(1)*} \left( \chi_\pm^{(1)} + \chi_\mp^{(1)} \right)^*. \quad (\text{S57})$$

The linear term in  $g_0$  describes the contribution of the optomechanical coupling to the linear modulation of the mechanical motion, while the cubic term in  $g_0$  describes the induced nonlinear modulation. The real and imaginary parts of these coefficients represent contributions to the mechanical resonance frequency and damping rate, respectively. Using the expression of the intracavity intensity,

$$|a(t)|^2 = n_{\text{cav}}(\Delta) |E(t)|^2, \quad (\text{S58})$$

we can rewrite the third terms of the right-hand side in Eq. (S21) as

$$\begin{aligned} ig_0 |a(t)|^2 e^{-i\Omega_m t} &= in_{\text{cav}}(\Delta) g_0 |E(t)|^2 e^{-i\Omega_m t} \\ &= -in_{\text{cav}}(\Delta) g_0^2 \left( C_1(\Delta) B(t) + g_0^2 (C_2(\Delta) + C_3(\Delta) + C_4(\Delta)) |B|^2 B(t) \right) e^{-i\Omega_m t} \\ &= -in_{\text{cav}}(\Delta) g_0^2 \left( C_1(\Delta) b(t) + g_0^2 (C_2(\Delta) + C_3(\Delta) + C_4(\Delta)) |b|^2 b(t) \right). \end{aligned} \quad (\text{S59})$$

From the form of the equation of motion for the nonlinear oscillator [Eq. (S30)], the linear and nonlinear mechanical modulation terms originating from the optical force can be expressed as follows.

$$\dot{b}(t) = -i \left[ \Omega_{\text{eff}} - i \frac{\Gamma_{\text{eff}}}{2} \right] b(t) - i \left( \frac{3\alpha_{\text{opt}}}{2\Omega_m} - i \frac{\beta_{\text{opt}}}{2} \right) x_{\text{zpf}}^2 |b|^2 b(t) \quad (\text{S60})$$

$$\text{where } \Omega_{\text{eff}} = \Omega_m + \Omega_{\text{opt}}(\Delta), \quad \Gamma_{\text{eff}} = \Gamma_m + \Gamma_{\text{opt}}(\Delta) \quad (\text{S61})$$

Here, we obtain the optomechanically induced linear and nonlinear coefficients

$$\Omega_{\text{opt}}(\Delta) = n_{\text{cav}}(\Delta) g_0^2 \text{Re}[C_1(\Delta)] \quad (\text{S62})$$

$$\Gamma_{\text{opt}}(\Delta) = -2n_{\text{cav}}(\Delta) g_0^2 \text{Im}[C_1(\Delta)] \quad (\text{S63})$$

$$\alpha_{\text{opt}}(\Delta) = \frac{2\Omega_m}{3x_{\text{zpf}}^2} n_{\text{cav}}(\Delta) g_0^4 \text{Re}[C_2(\Delta) + C_3(\Delta) + C_4(\Delta)] \quad (\text{S64})$$

$$\beta_{\text{opt}}(\Delta) = -\frac{2}{x_{\text{zpf}}^2} n_{\text{cav}}(\Delta) g_0^4 \text{Im}[C_2(\Delta) + C_3(\Delta) + C_4(\Delta)], \quad (\text{S65})$$

where we use  $x_{\text{zpf}} = \sqrt{\frac{\hbar}{2m_{\text{eff}}\Omega_m}}$ . The ratio of the optomechanically induced nonlinear damping and Duffing coefficients is then given by

$$\frac{\beta_{\text{opt}}}{\alpha_{\text{opt}}}(\Delta) = -\frac{3}{\Omega_m} \frac{\text{Im}[C_2(\Delta) + C_3(\Delta) + C_4(\Delta)]}{\text{Re}[C_2(\Delta) + C_3(\Delta) + C_4(\Delta)]}. \quad (\text{S66})$$

Here, the specific parameter values used in the calculations are as follows. The effective mass is taken as  $m_{\text{eff}} = 7 \times 10^{-9}$  kg. This value is estimated by scaling from the effective mass of the radial breathing mode (RBM) of a microbottle resonator reported in Ref. [34]. The single-photon optomechanical coupling rate and the zero-point fluctuation amplitude are taken as  $g_0 = 2\pi \times 24$  Hz and  $x_{\text{zpf}} = 5.0 \times 10^{-18}$  m, respectively.

## OPTICALLY INDUCED MECHANICAL NONLINEARITY IN MULTI-MECHANICAL MODES

The intracavity photon mode depends on the displacements of all mechanical modes, as expressed in Eq. (S5). Its formal solution up to the third order in the optomechanical interaction is

$$\begin{aligned} \tilde{a}(t) = & \sqrt{\kappa_{\text{in}}} a_{\text{in}} \chi_0(\Delta) e^{-\lambda_0 t} + i \sqrt{\kappa_{\text{in}}} a_{\text{in}} \chi_0(\Delta) \sum_j g_j \int_{-\infty}^t q_j(s) e^{-\lambda_0 s} ds \\ & + i^2 \sqrt{\kappa_{\text{in}}} a_{\text{in}} \chi_0(\Delta) \sum_{j,k} g_j g_k \int_{-\infty}^t \int_{-\infty}^s q_j(s) q_k(s') e^{-\lambda_0 s'} ds ds' \\ & + i^3 \sqrt{\kappa_{\text{in}}} a_{\text{in}} \chi_0(\Delta) \sum_{j,k,l} g_j g_k g_l \int_{-\infty}^t \int_{-\infty}^s \int_{-\infty}^{s'} q_j(s) q_k(s') q_l(s'') e^{-\lambda_0 s''} ds ds' ds''. \end{aligned} \quad (\text{S67})$$

We assume that the displacement of the  $j$ -th mechanical mode can be written as a single-frequency vibration,  $\Omega_j$ , with a slowly varying complex envelope,  $B_j(t)$ ,

$$q_j(t) = B_j(t) e^{-i\Omega_j t} + \text{c.c.} \quad (\text{S68})$$

Substituting this expression into each nonlinear optomechanical term and performing the corresponding kernel integrals yields a generalized intracavity field that contains contributions from all mechanical modes. Inserting the resulting photon field into the radiation-pressure term then allows us to derive the optically induced mechanical nonlinearities for the multimode optomechanical system. Although the full expression becomes algebraically cumbersome, its structure parallels the single-mode result as shown in Eqs. (S62)-(S65). The real and imaginary parts of each optomechanical interaction term,  $J_1$ ,  $J_2$ , and  $J_3$ , govern the mechanically induced frequency shift and damping modification, respectively. Consequently, the radiation-pressure force acting on the  $j$ -th mechanical mode takes a form that depends on the amplitudes of all mechanical modes.

$$F_{\text{opt},j} = \hbar G_j |a(t)|^2 \propto - \left( \Omega_{\text{opt},j} + \sum_i \alpha_{ij} |b_i|^2 \right) b_j + i \left( \Gamma_{\text{opt},j} + \sum_i \beta_{ij} |b_i|^2 \right) b_j, \quad (\text{S69})$$

where  $\Omega_{\text{opt},j}$  and  $\Gamma_{\text{opt},j}$  denote the optically induced linear frequency shift and damping, respectively. Coefficients  $\alpha_{ij}$  and  $\beta_{ij}$  quantify the cross-nonlinear coupling between mechanical modes. As shown in Eq. (S69), once we consider multiple mechanical modes, the resonance frequency and the damping of a given mode become dependent on the amplitudes of the other mechanical modes. These cross terms give rise to cross-Duffing nonlinearity (frequency shift) and cross-nonlinear damping, respectively. The present formalism enables numerical estimation of all such coefficients.

## MEASUREMENT OF THERMAL MOTION OF MECHANICAL RBM IN THE MICROBOTTLE RESONATOR

We measured the thermal motion of the bottle-shaped optomechanical resonator fabricated on a silica optical fiber. The measurements were conducted under ambient-pressure and room-temperature conditions. Figure S1 shows a schematic of the experimental configuration used to measure the thermal motion. A laser with a wavelength near 1550 nm is launched into the bottle resonator through a tapered fiber (diameter  $\sim 1 \mu\text{m}$ ) with the thermally driven RBM to be transduced into intensity fluctuations of the transmitted optical signal, which are subsequently converted into a vibration spectrum using a spectrum analyzer (SA). In addition, the thermal-noise spectra obtained by the above procedure are used to calibrate the amplitude of the mechanical displacement. This calibration allows us to convert the measured voltage signals such as those obtained in the ring-down experiment shown in Fig. 2(b) in the main text into absolute displacement units *e.g.*, picometers.

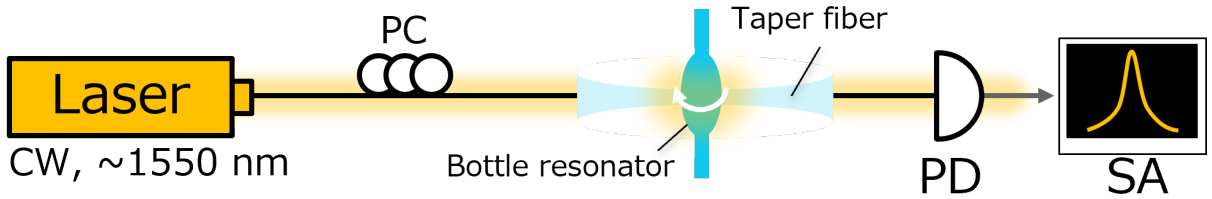


FIG. S1. Overview of experimental configuration. PC: Polarization controller, PD: Photodetector, SA: Spectrum analyzer.

The measured thermal-noise spectrum is shown in Fig. S2. From the Lorentzian fit, we obtain the peak amplitude of  $5.13 \mu\text{V}$  and the mechanical resonance frequency of  $\Omega_m = 2\pi \times 48.27 \text{ MHz}$ . Because thermal energy  $k_B T$  is comparable to the kinetic energy of the mechanical oscillator, thermal displacement amplitude  $x_{\text{th}}$  can be estimated from

$$\begin{aligned} \frac{1}{2} m_{\text{eff}} \Omega_m^2 x_{\text{th}}^2 &\simeq k_B T \\ \Rightarrow x_{\text{th}} &\simeq \sqrt{\frac{2k_B T}{m_{\text{eff}} \Omega_m^2}}. \end{aligned} \quad (\text{S70})$$

Using the resonator temperature of  $T = 300 \text{ K}$  and the effective mass of  $m_{\text{eff}} = 7 \times 10^{-9} \text{ kg}$ , Eq. (S70) yields a thermal displacement amplitude of  $x_{\text{th}} = 3.59 \text{ fm}$ . Calibration factor  $\eta_{\text{calib}}$  is therefore

$$\eta_{\text{calib}} = \frac{3.59 \text{ fm}}{5.13 \mu\text{V}}. \quad (\text{S71})$$

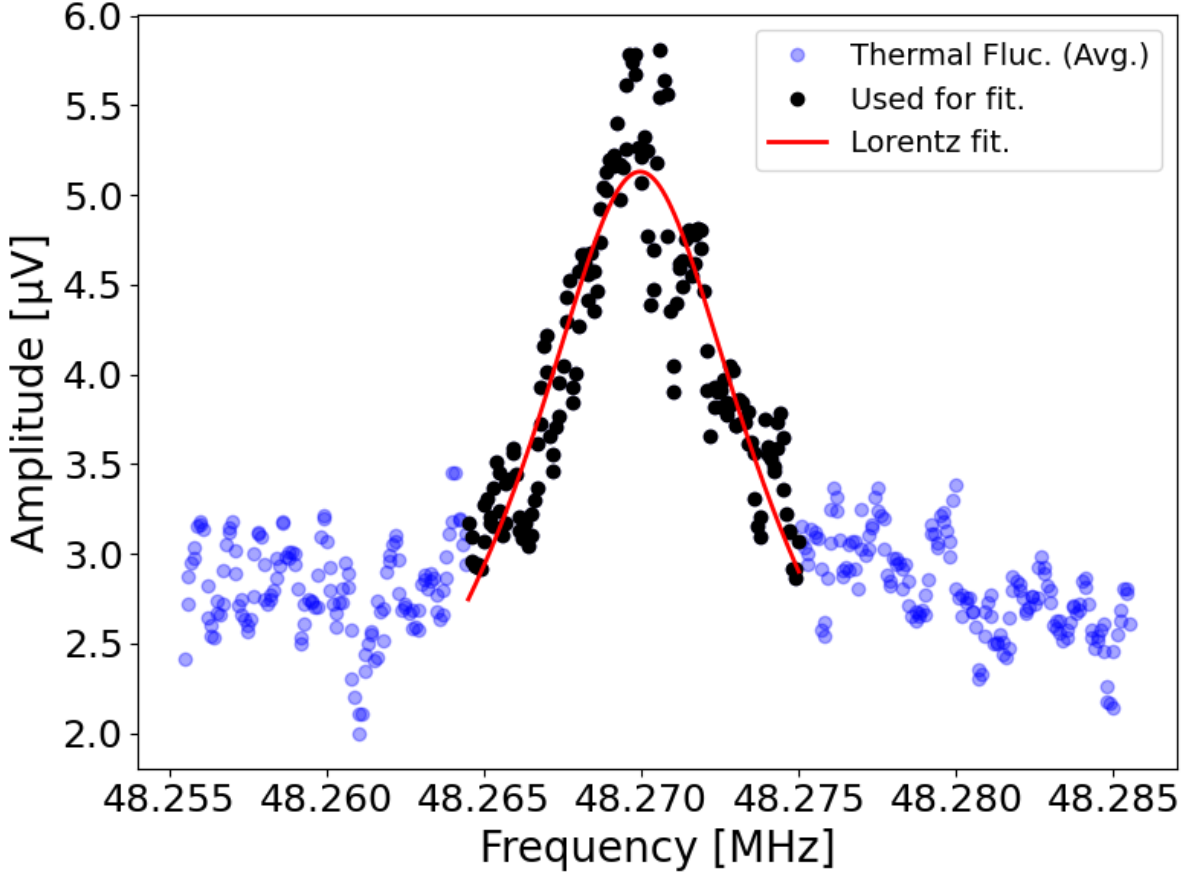


FIG. S2. Measured thermal-noise spectrum and its Lorentzian fit.

#### EXPERIMENTAL CONFIGURATION FOR PROBING OPTICALLY INDUCED MECHANICAL NONLINEARITY

In this section, we describe the experimental configuration used to measure the mechanical resonance spectra and ring-down dynamics of a single mechanical mode, as presented in Figs. 2 and 3 in the main text. As illustrated in Fig. S1, lasers are injected into the bottle resonator through evanescent coupling by setting a tapered fiber in contact with the bottle surface. For the excitation and detection of mechanical motion, we prepare two lasers with slightly different wavelengths: a pump laser ( $\sim 1550$  nm) for driving the mechanical RBM, and a probe laser ( $\sim 1520$  nm) for monitoring it. The pump laser is intensity-modulated using an electro-optic modulator, with a sinusoidal voltage of amplitude  $V$  and angular frequency  $\omega_{\text{mod}}$  generated by an arbitrary function generator. In this way, we periodically modulate the radiation pressure force, and resonantly drive the mechanical RBM by driving the modulation near the mechanical resonance ( $\omega_{\text{mod}} \sim \Omega_m$ ). We also tune the modulation depth of the pump intensity and, hence the excitation strength, by the applied voltage. The transmitted pump and probe lasers pass through the cavity, after which the pump is filtered out by a bandpass filter (BPF), and the remaining probe is detected by a lock-in amplifier for mechanical readout.

To investigate the nonlinear mechanical behavior induced by optomechanical coupling, we inject a strong optical field into the cavity so that the radiation-pressure force acquires a nonlinear dependence on the mechanical displacement. As the intracavity photon number increases, higher-order components of the optical force become significant giving rise to optically induced Duffing nonlinearity and nonlinear damping. In the experiments, the pump beam was amplified to an optical power of approximately 50 mW before entering the cavity [Fig. S3], enabling access to the nonlinear regime. In the nonadiabatic regime, where the cavity response time is comparable to the mechanical oscillation period, the delayed optical backaction produces an effective damping force that depends on the vibrational amplitude.

Since the modulation frequency is much higher than the mechanical damping rate ( $\omega_{\text{mod}} \gg \Gamma_m$ ), the mechanical

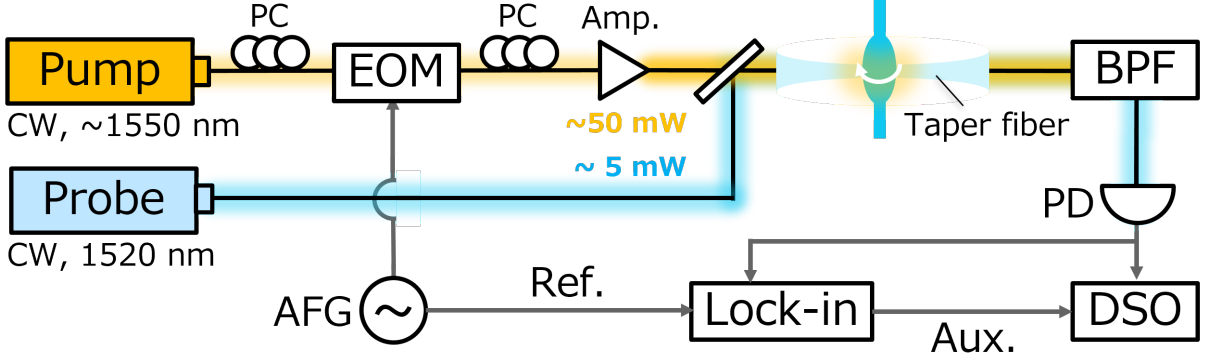


FIG. S3. Experimental configuration. EOM: Electro-optic modulator, AFG: Arbitrary function generator, BPF: Bandpass filter, DSO: Digital sampling oscilloscope, PC: Polarization controller, PD: Photodetector.

oscillator responds to the time-averaged optical force. Taking into account the nonadiabatic nonlinearity of the optical force, the equation of motion for the mechanical oscillator can be written as follows.

$$\ddot{x} + (\Gamma_m + \beta_{\text{opt}}x^2) \dot{x} + (\Omega_m^2 + \alpha_{\text{opt}}x^2) x = \frac{F_d}{m_{\text{eff}}} \cos(\omega_{\text{mod}}t), \quad (\text{S72})$$

where  $\Gamma_m$  and  $\Omega_m$ , respectively, denote the mechanical damping and resonance frequency including the modulation induced by the linear optomechanical coupling, and  $F_d$  represents the amplitude of the driving force induced by the optical force.

## THEORETICAL ESTIMATION OF MECHANICAL GEOMETRIC NONLINEARITY

Here we discuss the derivation of Duffing nonlinearity  $\alpha_G$  originating from the geometric deformation for the fundamental RBM in the microbottle structure given by

$$u_r(r, z) = -k_r J_1(k_r r) H_0(\sqrt{k_0 \beta} z) \exp\left[-\frac{k_0 \beta}{2} z^2\right], \quad (\text{S73})$$

$$u_z(r, z) = -2k_0 \beta z J_0(k_r r) \exp\left[-\frac{k_0 \beta}{2} z^2\right], \quad (\text{S74})$$

where  $k_r = 1.84/R_0$  is the main radius of the microbottle,  $k_0 = \sqrt{k_r^2 + \beta^2} + \beta$  is the curvature of  $\beta$  parameterizing the shape of the microbottle, and  $r(z) = \sqrt{1 + \beta^2 z^2} R_0$ . Terms  $J_n(x)$  and  $H_n(x)$  denote the  $n$ th order of the Bessel function and Hermite polynomial, respectively.

The mechanical strain generalized by the structural deformation can be given by the Green-Lagrange strain,  $E = \frac{1}{2}(FF^t - I)$ , where  $F$  shows the deformation tensor given by

$$F = \begin{pmatrix} 1 + u_{r,r} & 0 & u_{r,z} \\ 0 & 1 + u_r/r & 0 \\ u_{z,r} & 0 & 1 + u_{z,z} \end{pmatrix}, \quad (\text{S75})$$

with  $u_{i,j} \equiv \partial_j u_i$ . In order to estimate roughly the order of the nonlinear coefficient, we avoid the derivatives and keep only  $u_r/r$ . Furthermore, we avoid  $u_z$ , which is much smaller than  $u_r$  in the conventional RBM. Thus, the equation of motion is given by

$$\rho \ddot{u}_r = \nabla \sigma = \nabla \left( \frac{1}{|F|} FS F^t \right), \quad (\text{S76})$$

$$S_{ij} = \lambda(\text{Tr}[E])\delta_{ij} + 2\mu E_{ij}, \quad (\text{S77})$$

where  $\lambda$  and  $\mu$  are Lamé constants. It can be approximated to

$$\rho \ddot{u}_r = -E_0 \frac{u_r}{r^2} - 2E_0 \frac{u_r^3}{r^4} + \mathcal{O}(u_r^2, u_r^4), \quad (\text{S78})$$

where  $E_0 = \lambda + 2\mu$  is the Young modulus, and  $\mathcal{O}(u_r^2, u_r^4)$  denotes the second- and fourth-order terms that do not affect the rotating dynamics in the mechanical mode. This equation can be transformed to the mode equation via decomposition  $u_r(r, z, t) = \phi_r(r, z)U(t)$  with  $\max_{r,z} |\phi_r(r, z)| = 1$ . Finally, we obtain

$$\ddot{U} = -\Omega^2 U + \alpha_G U^3 \quad (\text{S79})$$

with

$$\alpha = \frac{2E}{m_{\text{eff}}} \int \frac{\phi_r^4}{r^4} dV, \quad (\text{S80})$$

$$m_{\text{eff}} = \rho_0 \int \phi_r^2(r) dV. \quad (\text{S81})$$

By using the practical parameters in our device,  $R_0 = 40 \mu\text{m}$ ,  $\beta = 625 \text{ m}^{-1}$ ,  $\rho_0 = 2648 \text{ kg/m}^3$ ,  $E_0 = 72 \text{ GPa}$ , we estimate  $\alpha_G = 6.3 \times 10^{25} \text{ m}^{-2}\text{s}^{-2}$ , which is eight orders of magnitude smaller than  $\alpha_{\text{OM}}$ . Such a small geometrical nonlinearity is consistent because of the small deformation in the RBMs.

## FITTING EQUATION FOR RING-DOWN WITH NONLINEAR DAMPING

To derive the ring-down dynamics in the presence of nonlinear damping, we begin with the forced nonlinear oscillator

$$\ddot{x} + (\Gamma_m + \beta x^2) \dot{x} + \Omega_m^2 x = F \cos(\omega t). \quad (\text{S82})$$

After the external drive is switched off ( $F = 0$ ), the equation of motion reduces to

$$\ddot{x} + (\Gamma_m + \beta x^2) \dot{x} + \Omega_m^2 x = 0. \quad (\text{S83})$$

This describes a free harmonic oscillator with intrinsic linear damping  $\Gamma_m$  and amplitude-dependent nonlinear damping  $\beta x^2$ . Assuming weak nonlinearity ( $\beta$  small), the motion can be represented by slowly varying envelope form

$$x(t) = B(t) e^{-i\Omega_m t} + \text{c.c.}, \quad (\text{S84})$$

where envelope  $B(t)$  satisfies  $\dot{B} \ll \Omega_m B$  and  $\ddot{B} \ll \Omega_m \dot{B}$ . Under this approximation,  $\dot{x}(t)$  and  $\ddot{x}(t)$  are, respectively, given by

$$\begin{aligned} \dot{x}(t) &= (\dot{B} - i\Omega_m B) e^{-i\Omega_m t} + \text{c.c.}, \\ \ddot{x}(t) &= (\ddot{B} - 2i\Omega_m \dot{B} - \Omega_m^2 B) e^{-i\Omega_m t} + \text{c.c.} \end{aligned} \quad (\text{S85})$$

For the nonlinear damping term, we have

$$x^2 \dot{x} = \left( B^2 e^{-2i\Omega_m t} + 2|B|^2 + B_i^{*2} e^{2i\Omega_m t} \right) \left[ (\dot{B} - i\Omega_m B) e^{-i\Omega_m t} + \text{c.c.} \right]. \quad (\text{S86})$$

Extracting the resonance (positive-frequency) component yields

$$x^2 \dot{x} \big|_+ = 2|B|^2 (\dot{B} - i\Omega_m B) e^{-i\Omega_m t} + B^2 e^{-2i\Omega_m t} (\dot{B}^* + i\Omega_m B^*) e^{i\Omega_m t}, \quad (\text{S87})$$

then the dominant slowly varying component becomes

$$x^2 \dot{x} \big|_+ \approx -i\Omega_m |B|^2 B e^{-i\Omega_m t}. \quad (\text{S88})$$

The nonlinear envelope equation can be rewritten as

$$\dot{B} = -\frac{\Gamma_m}{2} - \frac{\beta}{2} |B|^2 B. \quad (\text{S89})$$

Next, we rewrite the real displacement in terms of a complex envelope as

$$x(t) = B(t) e^{-i\Omega_m t} + \text{c.c.}, \quad (\text{S90})$$

which guarantees that  $x(t)$  is real. On the other hand, the same motion can be written in real-amplitude form as

$$x(t) = b(t) \cos(\Omega_m t + \phi(t)). \quad (\text{S91})$$

Using  $\cos \theta = (e^{i\theta} + e^{-i\theta})/2$  and comparing Eqs. (S90) and (S91), we identify

$$B(t) = \frac{b(t)}{2} e^{-i\phi(t)}. \quad (\text{S92})$$

Therefore, real oscillation amplitude  $b(t)$  and the modulus of the complex envelope,  $B(t)$ , are related by

$$b(t) = 2|B(t)|. \quad (\text{S93})$$

In the following, we use Eq. (S93) to convert the envelope equation derived for  $B(t)$  into the fitting function for the experimentally measured real amplitude,  $b(t)$ . We obtain the envelope equation

$$\dot{b}(t) = -\frac{1}{2} \Gamma_m b(t) - \frac{1}{8} \beta b^3(t). \quad (\text{S94})$$

Let  $\Gamma'_m = \Gamma_m/2$  and  $\beta' = \beta/8$ . Then Eq. (S94) becomes

$$\frac{db(t)}{dt} = -\Gamma'_m b(t) - \beta' b^3(t). \quad (\text{S95})$$

Separating variables yields

$$\frac{db}{(\Gamma'_m + \beta' b^2)b} = -dt. \quad (\text{S96})$$

Using partial-fraction decomposition,

$$\int \frac{db}{(\Gamma'_m + \beta' b^2)b} = \frac{1}{\Gamma'_m} \ln b - \frac{1}{2\Gamma'_m} \ln(\Gamma'_m + \beta' b^2) + C_1. \quad (\text{S97})$$

Integrating Eq. (S96) gives

$$\frac{1}{2\Gamma'_m} \ln\left(\frac{b^2}{\Gamma'_m + \beta' b^2}\right) = -t + C. \quad (\text{S98})$$

Exponentiating,

$$\frac{b^2}{\Gamma'_m + \beta' b^2} = C'' e^{-2\Gamma'_m t}. \quad (\text{S99})$$

Applying initial condition  $b(0) = b_0$ ,

$$b^2(t) = \frac{b_0^2 e^{-2\Gamma'_m t}}{1 + (\beta' b_0^2 / \Gamma'_m) (1 - e^{-2\Gamma'_m t})}. \quad (\text{S100})$$

Thus the amplitude envelope becomes

$$b(t) = \frac{b_0 e^{-\Gamma'_m t}}{\sqrt{1 + (\beta' b_0^2 / \Gamma'_m) (1 - e^{-2\Gamma'_m t})}}. \quad (\text{S101})$$

Re-substituting  $\Gamma'_m = \Gamma_m/2$  and  $\beta' = \beta/8$ , we obtain the final fitting formula used in the analysis:

$$b(t) = \frac{b_0 e^{-\frac{\Gamma_m}{2} t}}{\sqrt{1 + \frac{\beta b_0^2}{4\Gamma_m} (1 - e^{-\Gamma_m t})}}. \quad (\text{S102})$$

Equation (S102) captures both the linear exponential decay at small amplitude and the enhanced decay due to nonlinear damping at large amplitude, and is used to fit the mechanical ring-down data.